Coincident biogenic nitrite and pH maxima arise in the upper anoxic layer in the Eastern Tropical North Pacific

Timur Cinay[1,3,*], Diana Dumit[1,3], Ryan J. Woosley[1], Elisabeth L. Boles[1,†], Jarek V. Kwiecinski[1,††], Susan Mullen[1,‡], Tyler J. Tamasi[1], Martin J. Wolf[1,‡‡], Colette L. Kelly[2], Nicole M. Travis[2], Karen L. Casciotti[2], Andrew R. Babbin[1,*]

[1] Department of Earth, Atmospheric and Planetary Sciences, Massachusetts Institute of Technology, Cambridge, MA, 02139, USA

[2] Department of Earth System Science, Stanford University, Stanford, CA, 94305, USA

[3] The authors contributed equally: Timur Cinay and Diana Dumit

[†] Now at the Department of Civil and Environmental Engineering, Stanford University, Stanford, CA, 94305, USA

[††] Now at the Division of Geological and Planetary Sciences, California Institute of Technology, Pasadena, CA, 91125, USA

[‡] Now at the Department of Earth and Planetary Science, University of California, Berkeley, Berkeley, CA, 94720, USA

[‡‡] Now at the Center for Environmental Law and Policy, Yale University, New Haven, CT, 06520, USA

* Correspondence to tcinay@mit.edu and babbin@mit.edu

Key Points

1. Secondary nitrite and pH maxima emerge in the oxygen deficient zone's upper anoxic core, overlaying a distinct tertiary nitrite maximum.
2. Anammox is the dominant mechanism for bioavailable nitrogen loss, and its relative rate is dependent on organic matter composition.
3. Denitrification of nitrite is the primary driver of the pH increase in the uppermost anoxic layers.

Abstract

The Eastern Tropical North Pacific (ETNP), like the other marine oxygen deficient zones (ODZs), is characterized by an anoxic water column, nitrite accumulation at the anoxic core, and fixed nitrogen loss via nitrite reduction to N_2O and N_2 gases. Here, we constrain the relative contribution of biogeochemical processes to observable features such as the secondary nitrite maximum (SNM) and local pH maximum by simultaneous measurement of inorganic nitrogen and carbon species. High-resolution sampling within the top 1 km of the water column reveals consistent chemical features previously unobserved in the region, including a tertiary nitrite maximum. Dissolved inorganic carbon measurements show that pH increases with depth at the top of the ODZ, peaking at the potential density of the SNM at σ_θ = 26.15 ± 0.06 (1 s.d.). We developed a novel method to determine the relative contributions of anaerobic ammonium oxidation (anammox), denitrification, nitrite oxidation, dissimilatory nitrate reduction to nitrite, and calcium carbonate dissolution to the nitrite cycling in the anoxic ODZ core. The calculated relative contributions of each reaction are slightly sensitive to the assumed C:N:P ratio and the carbon oxidation state of the organic matter sinking through the ODZ. Furthermore, we identify the source of the pH increase at the top of ODZ as the net consumption of protons via nitrite reduction to N_2 by the denitrification process. The increase in pH due to denitrification impacts the buffering effect of calcite and aragonite dissolving in the ETNP.

1. Introduction

Marine oxygen deficient zones (ODZs) play a significant role in the global nitrogen cycle by removing 30-50% of fixed nitrogen in the ocean, even though they comprise less than 0.1% of the ocean's volume (Brandes & Devol, 2002; Codispoti et al., 2001; DeVries et al., 2013; Gruber & Sarmiento, 1997; Karstensen et al., 2008). The Eastern Tropical North Pacific (ETNP) off Mexico and Central America is one of the three largest permanent ODZs (Kwiecinski & Babbin, 2021; Paulmier & Ruiz-Pino, 2009). The ETNP is characterized by highly productive coastal regions due to nutrient supply by the coastal upwelling (López-Sandoval et al., 2009; Stramma et al., 2010) and a large region of low-oxygen water column overlaid by predominantly oligotrophic surface ocean (Fuchsman, Palevsky, et al., 2019; Pennington et al., 2006). Below a

well-mixed surface layer, oxygen concentrations decrease to levels as low as 10 nmol L^{-1} (Morrison et al., 1998; Revsbech et al., 2009; Thamdrup et al., 2012; Tiano et al., 2014), corresponding to aerobic subsistence concentrations at which anaerobic metabolism can coexist with or dominate over aerobic respiration (Zakem & Follows, 2017).

Nitrite (NO_2^-) is a central dissolved inorganic nitrogen (DIN) compound in the ODZ nitrogen cycle because it is a product or reactant for denitrification, anammox, and recycling of nitrate via dissimilatory nitrate reduction to nitrite (DNRN) and nitrite oxidation (Figure 1). A nitrate deficit and a similar magnitude excess of dissolved dinitrogen gas (N_2) concentrations in the ETNP implies the reduction of nitrite in the ODZ and consequential removal of the DIN (Chang et al., 2012; Fuchsman et al., 2018). Removal of biologically available DIN in ODZs is typically performed by either a heterotrophic denitrification process or autotrophic anaerobic ammonium oxidation (anammox) reaction (Babbin et al., 2014; Bristow et al., 2016; Ward, 2013). The proportion of nitrogen loss via denitrification and anammox, respectively, in the anoxic water column, and the complexity of the complementary metabolisms that support them, remain unresolved, particularly when considering the ODZ not as a uniform system but as a complex combination of multiple isopycnal layers and water masses. While some studies suggest that, on a whole, anammox is the dominant production pathway for N_2 in the ODZ (Babbin et al., 2017; Kalvelage et al., 2013), others report that denitrification exceeds anammox in anoxic environments (Dalsgaard et al., 2012; Ward et al., 2009). Since denitrification and DNRN generate ammonium used in anammox (Figure 1), anammox would account for approximately 30% of N_2 production in the ODZ solely based on reaction stoichiometry for canonical organic matter composition (Devol, 2003). However, variations in the organic matter composition (Babbin et al., 2014), differences in the oxygen inhibition of denitrification and anammox reactions (Dalsgaard et al., 2014), or existence of other metabolisms (Babbin, Buchwald, et al., 2020; Lam et al., 2009) could alter the proportion N_2 production attributable to anammox. Elucidating the denitrification-anammox dichotomy is critical for understanding the connection between the global nitrogen cycle and climate. Denitrification is a significant marine natural source of nitrous oxide (N_2O) (Babbin et al., 2020; Babbin et al., 2015; Ji et al., 2015),

which is a key greenhouse gas and stratospheric ozone-depleting substance in the atmosphere (Naqvi et al., 2000; Ravishankara et al., 2009). In addition, anammox and denitrification have a differential impact on dissolved inorganic carbon (DIC) chemistry because autotrophic processes such as anammox consume DIC, whereas heterotrophic processes such as denitrification release DIC. Denitrification can admittedly also occur as an autotropic process involving the sulfur redox chemistry (Fuchsman et al., 2017; Raven et al., 2021; Saunders et al., 2019), or methane oxidation (Thamdrup et al., 2019). However, in ODZs autotrophic denitrification is less significant compared to heterotrophic denitrification, so it is neglected in this study. Furthermore, recent studies assessing anammox and denitrification rates with incubation experiments suggest that the organic matter (OM) supply and composition play a critical role in the relative contributions of anammox and denitrification to nitrogen loss (Babbin et al., 2014; Chang et al., 2014; Ganesh et al., 2015; Kalvelage et al., 2013; Ward, 2013).

[Figure 1]

Nitrite profiles in ODZs differ markedly from the oxygenated global ocean. In the ODZs, nitrite accumulates in the water column at two distinct horizons: (i) the primary nitrite maximum (PNM) at the base of the euphotic zone, which also occurs globally, and (ii) the secondary nitrite maximum in the anoxic core, which is restricted to ODZs (Brandhorst, 1959; Buchwald et al., 2015; Buchwald & Casciotti, 2013; Lipschultz et al., 1996). The formation of the PNM is typically related to light-limited phytoplankton assimilation of nitrate or an imbalance of aerobic ammonium and nitrite oxidation (Buchwald & Casciotti, 2013; Lomas & Lipschultz, 2006; Zakem et al., 2018) and is outside the scope of this article. Nitrite accumulation in the anoxic core results from the rate differences between nitrite sources, i.e., dissimilatory nitrate reduction to nitrite (DNRN), and sinks, i.e., nitrite reduction via denitrification or anammox and nitrite (re)oxidation. Both direct rate measurements of denitrification and natural abundance isotopic analyses report that rapid recycling of nitrate (NO_3^-) and nitrite by DNRN and nitrite oxidation is dominant compared to nitrite reduction at the top of the ODZ (Babbin et al., 2017; Buchwald et al., 2015; Füssel et al., 2012; Kalvelage et al., 2013; Peters et al., 2016). Since the discovery of nitrite oxidation in the ODZs (Füssel et al., 2012),

multiple studies have attempted to provide a possible mechanism for nitrite oxidation in the anoxic core, such as intrusion of oxygenated water masses (Bristow et al., 2016; Tsementzi et al., 2016), oxygen production by *Prochlorococcus* (Garcia-Robledo et al., 2017), oxidation by iodate and metals (Babbin et al., 2017; Evans et al., 2020; Hardisty et al., 2021; Moriyasu et al., 2020), nitrite dismutation (Babbin, Buchwald, et al., 2020) and anaerobic nitrite oxidation by anammox bacteria (Brunner et al., 2013). Understanding the relative distribution of nitrite oxidation in the ODZ core can significantly improve the understanding of the source and mechanism of nitrite oxidation.

Marine ODZs also exhibit unique inorganic carbon chemistry compared to the oxygenated pelagic ocean, containing, for instance, some of the lowest pH waters in the open ocean and correspondingly shallowest aragonite and calcite saturation horizons (Hernandez-Ayon et al., 2019; Jiang et al., 2019; Millero, 2007). Due to the long residence time accumulating remineralization products, these waters contain very high dissolved inorganic carbon (DIC) resulting from aerobic respiration and correspondingly low pH. High DIC concentrations up to 2350 μmol kg^{-1} and in-situ pH (total scale) values below 7.5 at 50 m depth have previously been reported in the Eastern Tropical South Pacific ODZ (Hernandez-Ayon et al., 2019; Paulmier et al., 2011), and similar features such as approximately 2300 μmol kg^{-1} DIC and pH below 7.6 are observed in historical data, such as the P18 WOCE section sampled during CLIVAR and GO-SHIP, from the ETNP (Lauvset et al., 2021; Olsen et al., 2020). Calcite and aragonite are calcium carbonate ($CaCO_3$) minerals produced by phytoplankton such as coccolithophores, zooplankton such as pteropods, and protozoans such as foraminifera. The dissolution of calcium carbonate has a buffering effect on ocean acidification, impacts the ocean's ability to absorb CO_2 from the atmosphere (Feely et al., 2002), and acts to ballast sinking organic material. Furthermore, in-situ pH conditions are thought to affect the dissolution of biogenic $CaCO_3$ particles by impacting the DIC speciation and CO_3^{2-} concentrations in the water column (Millero, 2007). Classically, saturation state (Ω) has been defined to indicate a thermodynamic tendency for calcium carbonate to precipitate ($\Omega > 1$) or dissolve ($\Omega < 1$). However, the dissolution of $CaCO_3$ cannot be simplified to just ambient pH, and saturation conditions as prior studies suggest that mineral

151 structure and other biogeochemical dynamics play significant roles in modifying
152 dissolution kinetics and distribution (Adkins et al., 2021; Milliman et al., 1999; Pan et al.,
153 2021; Subhas et al., 2022; Woosley et al., 2012). Consequential to low pH, aragonite
154 saturation horizon depths (where $\Omega = 1$, see Equation 6) shallower than 100 m are
155 notably observed in ODZs (Feely et al., 2002; Hernandez-Ayon et al., 2019).

156 Even though inorganic nitrogen and carbon chemistry in the ODZs are
157 interconnected, there are few data from ODZs examining the inter-related cycling of
158 these elements or investigating the impact of denitrification on pH in these waters. While
159 denitrification of nitrite accompanied by the respiration of sinking organic matter in
160 ODZs releases CO_2, potentially decreasing pH, it also consumes protons and produces
161 alkalinity (Koeve & Kähler, 2010), which can counterbalance the pH decrease. In
162 addition, sulfate reduction (Jørgensen, 1982; Raven et al., 2021) and particle- or
163 zooplankton-associated methanogenesis (Sasakawa et al., 2008; Schmale et al., 2018)
164 can impact the biogeochemistry in the ODZ. However, the contributions from such
165 processes are typically negligible in comparison to nitrogen metabolisms (Raven et al.,
166 2021; Schmale et al., 2018) and excluded from this analysis of the major
167 biogeochemical pathways. Understanding the interrelated cycling of DIN and DIC
168 requires simultaneous and spatially high-resolution measurements that can reveal sharp
169 chemical gradients in the ODZs. High-resolution measurements ensure that the critical
170 features such as local extrema or large vertical changes in nutrient and pH profiles are
171 accurately represented so that the critical link between DIN and DIC cycles can be
172 resolved.

173 Here, we present a novel framework for studying ODZ biogeochemistry and the
174 nitrogen cycle, focusing on nitrite accumulation and pH increase across the broad SNM
175 by investigating the coupling between inorganic carbon chemistry and the nitrogen cycle
176 based on in-situ biogeochemical measurements. Although prior process-based studies
177 focus intensively on the ODZ nitrogen cycle with DIN measurements and by determining
178 reaction rates from incubation experiments, they generally overlook DIC measurements
179 and the role of pH in ODZ biogeochemistry. Such studies require perturbation or
180 stimulation of natural populations and potentially indicate current local conditions alone
181 (Dalsgaard et al., 2012; Ward et al., 2009). On the other hand, simultaneous DIC and

DIN geochemical measurements represent the integrated net changes in a water parcel moving along an isopycnal surface within the ODZ over time. Therefore, a new term, relative contribution, is introduced in this study to represent the net effect of cumulative biogeochemical metabolisms in the ETNP ODZ. Relative contribution refers to the proportional effect metabolic reactions have in producing or consuming a shared reference tracer. For example, the relative contribution of anammox, compared to denitrification, is the proportion of fixed nitrogen lost via anammox relative to the total N_2 production by anammox and denitrification combined. We assess the relative contribution of key reactions, including DNRN, nitrite oxidation, nitrite reduction to N_2 via canonical heterotrophic denitrification (referred to as denitrification from this point onward), anammox, and calcium carbonate dissolution by constraining observed changes in DIN and DIC concentrations and speciation. Building on prior work, we investigate the correlation between the relative contribution and organic matter content by varying the carbon oxidation state and C:N:P ratio in a model framework based on literature values. Lastly, we compare observations to a hypothetical water pH profile to investigate the impact of denitrification on observed pH in the ETNP ODZ and $CaCO_3$ saturation state in the water column.

2. Methods

2.1. Sample collection, tracer measurements, and data analysis

The present study focuses on data collected during a research cruise on *R/V Falkor* (FK180624) in the Eastern Tropical North Pacific (ETNP) in June–July 2018. Additionally, nitrite, pH, alkalinity, and oxygen data from the AT37-12 cruise on *R/V Atlantis* in the southern part of the ETNP in April–May 2017 are presented as supplemental information. Samples at various depths were acquired using a 24-bottle CTD rosette equipped with temperature, salinity, pressure, and oxygen sensors at 19 stations while focusing on the upper 1 km during the FK180624 cruise (Figure 2). The same sample acquisition method was followed during AT37-12 for 8 stations (Figure S1). All stations mentioned in the main text and presented in the main figures belong to FK180624. AT37-12 data are presented for comparison in the supporting information.

Total alkalinity (TA) was collected in borosilicate glass bottles and poisoned immediately with 0.02% mercuric chloride. Samples were stored in the dark at room

temperature and measured in the lab following the cruise using a custom-designed open-cell titration system designed and built by the laboratory of Andrew G. Dickson (Scripps Institution of Oceanography) following best practices (Dickson et al., 2007). The pH was collected and poisoned in the same manner as TA but measured onboard within 6 hours of collection. A custom-designed automated spectrophotometric system similar to Carter et al., (2013) using an Agilent 8454 UV-Vis spectrophotometer was used to measure the pH on the total scale at 25°C with purified meta-cresol purple indicator provided by Robert H. Byrne (University of South Florida). More details of the system can be found in Woosley, (2021). Nitrite, ammonium, and phosphate measurements were made spectroscopically with a 10 cm quartz cell and Ocean Optics QE Pro spectrometer (Babbin et al., 2014; Strickland & Parsons, 1972). NO_x^- (total nitrite and nitrate) measurements were performed using a Teledyne T200 analyzer via the standard chemiluminescence protocol (Babbin & Ward, 2013; Braman & Hendrix, 1989).

[Figure 2]

Physical seawater properties such as potential temperature (θ), density (ρ), and potential density anomaly referenced to surface (σ_θ) were calculated using the TEOS-10 GSW package (Firing et al., 2021). Dissolved inorganic carbon (DIC) and in-situ pH calculations were done by $PyCO_2SYS$ package version 1.8 for Python 3.8 (Humphreys et al., 2020; Van Heuven et al., 2011). Dissociation constants K_1 and K_2 were based on Lueker et al., (2000). The total boron of Lee et al., (2010) and the K_{HF} of Perez and Fraga, (1987) were used.

2.2. Organic matter composition and reaction stoichiometry

The chemical composition of organic matter sinking to the ODZ during our occupation was estimated by calculating the relative changes in nutrient, DIC, and apparent oxygen utilization (AOU) along the oxycline surface across all 19 stations. Admittedly, relative changes in nutrients, DIC, and AOU are impacted by processes other than the organic matter remineralization such as vertical diffusion and lateral mixing. Therefore, determining the organic matter composition using relative changes in nutrients, DIC, and AOU in the oxycline surface is a simplification and estimate for this region at the time of sampling. Nevertheless, the sensitivity analyses in the later

sections with standard organic matter formulations show similar results. The oxycline was defined between 45–95 dbar pressure based on the water column oxygen profile (Figure S4a). The study focuses on stations 1–14, excluding station 5 for further analysis because (i) stations 5, 15, and 17 are impacted by mesoscale eddies that can alter the water column structure and chemistry (Figure S5) and (ii) stations 16, 18, and 19 have the lateral intrusion of oxygenated water masses at the top of ODZ (Figure S3a). These layers diverge from the canonical definition of the ODZ due to oxygen intrusion and have a different water column chemistry. DIC, DIN, and oxygen concentration data from the selected stations were fitted against phosphate concentration in the oxycline using robust regression with Huber's t M-estimation method available on the Scikit-learn package (Pedregosa et al., 2011). Huber's t robust regression assigns varying weight values to outliers based on the predicted residual values, reduces the contribution of outliers to the regression, and increases the accuracy of slope value (Huber, 1973).

Sinking organic matter (OM) composition was calculated from the resulting C:N:P ratio following Moreno et al. (2020) and Paulmier et al. (2009). Stoichiometric coefficients for remineralization of the OM via DNRN and denitrification (Koeve & Kähler, 2010) and autotrophic anammox reaction (Strous et al., 1998) were determined from previous studies. Generic nitrite oxidation to nitrate without prescribing a specific oxidant and the calcium carbonate dissolution reaction were added to the list of key reactions occurring within the ODZ (Table 1).

[Table 1]

The variables a–e in Table 1 refer to the elemental ratios of the organic matter remineralized in the ODZ. These variables are used to calculate stoichiometric coefficients of nitrate, nitrite (x and z), and water (y and w) in DNRN and denitrification reactions based on Koeve and Kähler (2010). Additionally, the (b – 2c) term refers to the hydrogen content of the organic matter with respect to the oxygen content. Since organic matter hydrogen and oxygen content cannot be assessed in our data, the (b – 2c) term was set by balancing the oxidation states for the organic matter. The C_{ox} term refers to the oxidation state of organic carbon and was calculated from the respiration quotient that describes the molar ratio of oxygen to organic carbon consumed during the

aerobic respiration (Moreno et al., 2020). Oxygen consumption to phosphate production ratio ($r_{AOU:P}$) in the oxycline was used to calculate C_{ox} because the respiration quotient is restricted to the amount of oxygen consumed by aerobic respiration and nitrification in oxic environments.

2.3. Relative reaction rates and relative contribution calculations

Based on the observed vertical oxygen, nitrite, and pH profiles, the suboxic ETNP water column ($25.0 < \sigma_\theta < 27.4$ kg m^{-3}) was divided into 16 layers (isopycnal surfaces) to calculate the relative contribution of 5 key reactions (DNRN, nitrite oxidation, denitrification, anammox, and calcium carbonate dissolution) to the biogeochemical cycling of DIN and DIC in the ODZ (Table S1). It is important to note that the anoxic core of the ODZ is narrower than the full range of 16 layers, typically covering only layers 3 - 14 (Figures 2c & S2). Initially, 8 layers were defined based on oxygen, nitrite, and pH data from stations 1–14, excluding station 5. Then, each layer was divided into 2 to capture the spatial resolution in the results while balancing the number of data points at each layer. For the 16 layers, the change in 5 tracer concentrations was calculated with respect to changes in DIC. The tracers were nitrate (NO_3^-), nitrite (NO_2^-), ammonium (NH_4^+), N*, and total alkalinity (TA). The quasi-conservative N* tracer refers to the relative DIN deficiency relative to phosphate based on the N:P ratio in the organic matter (Equation 1) (Deutsch et al., 2001; Gruber & Sarmiento, 1997).

$$N^* = ([NO_3^-] + [NO_2^-] + [NH_4^+]) - r_{N:P}[PO_4^{3-}] + 2.9\mu mol\ kg^{-1} \quad (1)$$

The tracer concentrations within a layer were plotted against DIC using Huber's t M-estimation method (Pedregosa et al., 2011), which accounts for outliers in each isopycnal layer separately. The slope of the regression fit is denoted as Δtracer (formally, this is the change in the tracer quantity normalized per unit change of DIC). Assuming Δtracer values are impacted only by the 5 key reactions in the ODZ, Δtracer is a linear combination of each tracer's stoichiometric coefficients in each reaction (Equation 2). Subscripts i refer to tracers, including DIC, and j refer to 5 key reactions. R is a 6-by-5 matrix that combines each tracer's stoichiometric coefficients and relative

reaction rates (referred to as χ in the following equations) varying by layer. All the terms in Equation 2, including the relative reaction rates in χ matrix, are unitless because no time proxy was measured in the study. An example calculation is provided in the supplemental information. Reaction coefficients were calculated by solving the linear system of equations using a non-negative least-squares method (scipy.optimize.nnls() function) available on Python SciPy package (Virtanen et al., 2020).

$$\Delta\, Tracer_i = \sum_j (R_{i,j} \times \chi_j) \quad (2)$$

Building upon the relative reaction rates, the relative contribution (RC) of each reaction in a particular layer is calculated with respect to a reference tracer. For example, (i) the relative contribution of denitrification and anammox reactions is calculated with respect to ΔNO_2^- (Equations 3 and 4). Expressions for the other relative contribution calculations are given in the supplemental information (Equations S1–S10)

$$RC_{denitrification} = \frac{R_{NO2,denitrification} \times \chi_{denitrification}}{R_{NO2,denitrification} \times \chi_{denitrification} + R_{NO2,anammox} \times \chi_{anammox}} \quad (3)$$

$$RC_{anammox} = 1 - RC_{denitrification} \quad (4)$$

The error in the relative reaction rates (χ) and RC values was assessed by Monte Carlo simulations (n = 10,000), as follows. A Δtracer value was randomly selected from the normal distribution defined based on the robust fit regression results, then used to calculate relative reaction rates and RC values as described above. χ and RC values are reported as the mean of 10,000 such simulations with one standard deviation (1 s.d.) of the simulation.

2.4. Expected ΔpH calculation in the presence of denitrification

Based on Table 1 and Table S2, denitrification consumes protons, hence increasing pH. However, CO_2 released due to denitrification speciates in the water column, releasing protons and decreasing pH. Overall, net proton consumption and pH increase is expected based on the denitrification stoichiometric coefficients (Table 1 and S2). To estimate the net pH increase (ΔpH) at the top of the ODZ due to denitrification, in-situ pH per organic carbon remineralized is calculated for an approximate range of total alkalinity (2200–2450 μmol kg^{-1}) and DIC (2000–2400 μmol kg^{-1}) observed in the ETNP based on GLODAP v2.2021 (Lauvset et al., 2021; Olsen et al., 2019, 2020). Some specific combinations plotted, e.g., low DIC and high total alkalinity or high DIC and low total alkalinity are unlikely to be observed. ΔpH represents the increase in pH

due to denitrification compared to a baseline case assuming no water-column denitrification. In-situ pH values are determined using the CO_2SYS package with set temperature (11 ºC), salinity (35), and pressure (300 dbar) inputs selected as representative values in the ETNP ODZ.

2.5. Water column pH and $CaCO_3$ saturation state

Observed in-situ pH data from the selected stations are fitted as a function of depth (z) between 50–900 dbar with a linear combination of exponential decay and Gaussian curve using ordinary least-squares (scipy.optimize.curve_fit() function) available on SciPy package (Equation 5) (Virtanen et al., 2020). Exponential decay is parameterized by an amplitude (*a*) and a decay coefficient (*b*). The Gaussian function is parameterized by the amplitude (*c*), mean (*d*), and spread (*e*) variables. Since pH values converge to a constant value rather than zero at depth, an additional constant (*f*) is also included. Then, a hypothetical pH curve is constructed with an exponential decay function that approximates a hypothetical pH profile with no local pH maximum arising from denitrification (i.e., pH reflects only oxygen concentrations).

$$pH = ae^{-bz} + ce^{-\frac{(z-d)^2}{2e^2}} + f \quad (5)$$

For both pH curves, calcite and aragonite saturation state (Ω) (Equation 6) were derived using pyCO_2SYS (Humphreys et al., 2020) for in-situ temperature, salinity, and pressure conditions in the ETNP ODZ.

$$\Omega = \frac{[Ca^{2+}][CO_3^{2-}]}{K_{sp}^{CaCO_3}} \quad (6)$$

3. Results

3.1. Oxygen, dissolved inorganic nitrogen, alkalinity, and pH profiles in the ETNP ODZ

[Figure 3]

Oxygen concentration data for the collection of stations suggest that the anoxic ODZ in the ETNP is located approximately between σ_θ = 25.50 – 26.67 kg m^{-3} potential density surfaces (Figure 2c). An intrusion of oxygenated water masses is also observable for stations 16 and 19. Based on the nitrite profiles for each station (Figure 3a) and the profile for the collection of stations, nitrite starts accumulating at layer 5 and peaks at σ_θ = 26.15 ± 0.06 kg m^{-3} (1 s.d.) initially and at σ_θ = 26.43 ± 0.06 kg m^{-3} (1 s.d.)

for a second time before nitrite is consumed as oxygen concentration starts increasing again. Due to the existence of a local nitrite minimum (LNM) in concentration at σ_θ = 26.27 ± 0.10 kg m^{-3} (1 s.d.), we define the upper peak as SNM and the lower peak as a tertiary nitrite maximum (TNM), although note that canonically the secondary nitrite maximum refers to the full swath of nitrite accumulation rather than an individual specific maximum. Furthermore, pH increases at the top of the ODZ (layers 3-6), coincident with the accumulation of nitrite, to a peak that coincides with the SNM (Figures 2c and 3b) except for stations where oxygen intrusions are observed (Figure S3). In a smaller subset of stations, such as station 9, an additional increase in pH is observed below the local pH maximum, coinciding with the LNM.

Furthermore, similar two-peaked nitrite profiles can be observed in the anoxic core of a previous ETNP occupation in 2017 (Figure S1). However, prominent oxygen intrusions observed around 200 m in the southernmost stations reduce the thickness of the anoxic core. A narrower ODZ and prominent oxygen intrusions have been previously reported in the southern ETNP (Kwiecinski & Babbin, 2021; Margolskee et al., 2019), and are responsible for differences in nitrite accumulation among different stations in that previous occupation. Notably, however, the local nitrite minimum with concentrations below detection in station 1 from the AT37-12 cruise is observed at the same depths of a small (<5 μmol kg^{-1}) oxygen intrusion.

[Figure 4]

Station 9 (14ºN, 110ºW) was selected as the representative station for the ETNP ODZ, because coincident nitrite and pH peaks are apparent in the upper ODZ core (Figure 4), and it can be compared to previously reported data along the P18 line at 110ºW. Furthermore, increases in nitrate, phosphate, and alkalinity with increasing density were observed at this station, likely due to organic matter remineralization and calcium carbonate dissolution. In addition, ammonium is depleted (maximum of 0.03 μmol kg^{-1}) in the ODZ, likely via autotrophic processes such as anammox, in agreement with previous studies (Widner et al., 2018). When compared to previous measurements (CLIVAR in 2007 and GOSHIP in 2016) at the same location (Figure 5), similar ranges of oxygen, nitrite, and pH are recorded. However, sparse sampling previously did not permit distinct SNM and TNM of similar magnitudes to be observed in these studies,

even though the density surface of the TNM aligns in all three cruises (Figure 5). Yet, the pH increase in the upper ODZ is apparent in both our and CLIVAR data. Local pH minima and maxima from both cruises are observed at the same density surfaces.

[Figure 5]

3.2. Organic matter composition and key reactions

Based on nutrient, oxygen, and DIC calculations in the oxycline, the C:N:P ratio was determined for this limited region at the time of sampling as 112.50±4.25: 11.40±0.34: 1 mol/mol (1 s.d). In addition, apparent oxygen utilization (AOU) normalized to phosphate OM content ($r_{AOU:P}$) was calculated as 107.47±0.97 mol/mol (1 s.d.). If we assume that all the ammonium released during the respiration of organic matter is converted into nitrate via nitrification, the carbon oxidation state (C_{ox}) associated with the organic matter is +0.99 for the calculated $r_{AOU:P}$. On the other hand, if no nitrification is performed in the oxycline and AOU only represents the respiration, C_{ox} becomes +0.18. Since the rates of nitrification or anammox are unknown, both endmembers for C_{ox} are examined. The results presented in the following sections correspond to C_{ox} of +0.99, and the results for C_{ox} of +0.18 are given in the supporting information. Even though the analysis does not provide the exact oxygen and hydrogen content of the organic matter in both cases, the relative number difference of oxygen-to-hydrogen in the OM can be used to determine stoichiometric coefficients in DNRN and denitrification reactions (Table 1 and Table S2). The amount of water produced is not reported for balanced DNRN and nitrite denitrification reactions, but the biological production of H_2O has a negligible effect on the seawater chemistry. Based on the balanced reactions given the sinking organic matter composition, the reaction matrix (R), which represents the net change in a tracer due to reaction, is developed and shown in Table 2.

[Table 2]

Since the specific nitrite oxidation mechanism is not yet resolved under anoxic conditions and is likely a combination of numerous pathways, a general reaction expression is used. A recent study of two marine nitrite-oxidizing bacteria (*Nitrospira moscoviencis* and *Nitrospina gracilis*) reports that 0.0216 moles of carbon are fixed via the reductive tricarboxylic acid (rTCA) cycle per mole of nitrite oxidized (Zhang et al., 2020). Therefore, a $\Delta DIC:\Delta NO_3^-$ of -1:46.296 is selected for the nitrite oxidation column

in the R matrix. With the R matrix given in Table 2, relative reaction rates are calculated by non-negative least squares solution for each layer (Figure S6).

3.3. Relative contributions of biogeochemical reactions

Using set reaction stoichiometries and the observed changes in our inorganic nutrient tracers with respect to inorganic carbon, we calculate the reaction relative contribution (RC) to describe the distributions of key reactions in the ODZ and their proportional effect on the budget of a tracer (Figure 6). In terms of the loss of bioavailable fixed nitrogen (i.e, N_2 production), anammox accounts for between 34.9 and 79.2%, depending on the specific ODZ layer. Higher values are observed at the SNM and the bottom of the ODZ. In the layers above and below the anoxic ODZ core, where oxygen is more abundant, anammox accounts for 98.5% of N_2 production compared with denitrification. Notably, the distribution of the denitrification and anammox reactions calculated here do not precisely agree with the findings from microbial studies in the region (Fuchsman et al., 2017), which suggest dominant denitrification over anammox at the top of the ODZ. The discrepancy can be attributed to the presence of denitrifying organisms on particles and differential activity by individual organisms. This distribution does agree well, however, with data from the direct incubations (Babbin, Buchwald, et al., 2020). From our calculations, the relative denitrification contribution peaks just below the local nitrite minimum (LNM, layer 9) with an RC of 65.1% compared to anammox. Yet, anammox and denitrification combining to reduce nitrite to dinitrogen are not generally the major consumption pathway for nitrite.

Nitrite oxidation typically accounts for over 80% of all nitrite consumption except just below the top of the ODZ and the LNM (layers 4 and 9). Yet, nitrite production via DNRN and its combined consumption from anammox, denitrification, and nitrite oxidation are typically close to balanced, with the slight net rate leading to the shape of the profiles observed. Indeed, the first step of canonical denitrification, DNRN, is always greater than denitrification from nitrite, supporting the concept of rapid recycling of nitrate in the ODZ. Comparing the rates of DNRN with nitrite oxidation directly, we find that nitrate reduction is between 1 and 10 times as large as nitrite oxidation, with peak DNRN to nitrite oxidation ratios at the top of the ODZ and just below the LNM, i.e., both depth zones where nitrite accumulates. Finally, in comparing the production of DIC

451 between net biological remineralization and calcium carbonate dissolution (Figure 6f),
452 the contribution of $CaCO_3$ dissolution decreases with depth between the top of the ODZ
453 and the LNM and increases below the LNM. $CaCO_3$ dissolution accounts for 15.5–
454 60.7% (but typically less than half) of DIC production in the ODZ, with a minimum in
455 layer 9, which is found to be a hotspot of denitrification.

[Figure 6]

456 *3.4. Variations in the organic matter carbon oxidation state and C:N:P ratio*

457 Since this study does not determine the amount of nitrification occurring in the
458 oxycline, total oxygen consumption during the aerobic remineralization of organic matter
459 is only partially constrained. Therefore, any organic matter C_{ox} value between the two
460 endmembers (+0.18 when no nitrification occurs and +0.99 when all the ammonium
461 from respiration is oxidized to nitrate) is possible within the study domain based on AOU
462 observations. However, the proposed C_{ox} values are outside the C_{ox} range observed
463 across the Eastern Pacific determined by Moreno et al., (2020). Moreno et al. (2020)
464 reports that the mean C_{ox} value in the ETNP along the P18 line (between ~10-20˚N) is -
465 0.76, although their full range spans -1.92 to -0.32 in the ETNP. Since a wide range of
466 oxidation states are reported, it is necessary to determine the effect of carbon oxidation
467 state on the relative contribution. We repeated the relative contribution calculations in all
468 16 layers in the ETNP ODZ for C_{ox} values ranging between -2.5 and +1.5 with 0.5
469 increments. The wider C_{ox} range was selected based on C_{ox} observed globally in
470 Moreno et al. (2020). In addition, we investigated the impact of C:N:P ratio on the
471 relative contribution of all the key reactions in the ODZ by repeating each calculation for
472 the Redfield C:N:P ratio (106:16:1)(Redfield, 1958) (Figure 7). The general vertical
473 pattern that suggests higher nitrite reduction at the top of the ODZ and the LNM did not
474 change when different C_{ox} and C:N:P ratios were used in the calculations (section 3.3,
475 Figure S7-9). However, the specific balance of anammox, denitrification, and nitrite
476 oxidation changed slightly for each layer, as shown in the supporting information and
477 illustrated as the range of values for anammox %, nitrite oxidation to reduction ratio, and
478 nitrite oxidation to DNRN ratio (Figure 7).

[Figure 7]

Anammox % (percentage loss of fixed nitrogen attributed to anammox), nitrite oxidation to reduction ratio, and nitrite oxidation to DNRN ratio are three critical values that show the impact of varying organic matter content on the relative contribution distribution by layer (Figure 7). Anammox % is mostly constant at different C_{ox} values except for at the top of the ODZ where the highest nitrite reduction contributions are observed. Therefore, we show that anammox % is strongly dependent on C_{ox} only at the top of the ODZ when C_{ox} is higher than zero. Anammox % for Redfield C:N:P ratio shows approximately a 10-17% increase compared to that for OM with observed C:N:P ratio (112.5:11.4:1 mol/mol) in all the layers due to an increase in organic nitrogen content. Moreover, the ratio of nitrite oxidation to reduction for the generic organic matter decreases with increasing $C_{ox,}$ and the change is more gradual at the top of ODZ compared to the other layers. Similarly, nitrite oxidation to DNRN ratio decreases with increasing C_{ox}, but more gradually for lower oxidation states. On the other hand, changing the C:N:P ratio does not vary the nitrite oxidation to reduction ratio and nitrite oxidation to DNRN ratio as much as anammox %.

Moreover, C_{ox} affects the pH increase relative to a baseline case with no denitrification at the top of the ODZ through changes in denitrification RC% (Figure 8). For OM with +0.99 carbon oxidation state, the increase in pH due to denitrification is calculated by taking the proton consumption, and DIC release into account (Table S2) at various alkalinity and DIC conditions in the water column (Figure 8a). Even though CO_2 is produced by the denitrification reaction, simultaneous consumption of protons balances the pH decrease due to DIC production. As a result, a net increase in pH is observed for the OM with +0.99 carbon oxidation state. For varying C_{ox} values, pH increase due to organic matter denitrification is observed below +1.27. On the other hand, other reactions, such as DNRN, consume fewer protons compared to those released via DIC production and result in a net pH decrease. Therefore, we can safely state that pH increase at the top of the ODZ signals nitrogen loss via denitrification of organic matter compositions reported in the ETNP ODZ because other key nitrogen cycle reactions cannot increase the pH.

[Figure 8]

3.5. pH and $CaCO_3$ saturation state

509 Observed pH values are fitted with a function of depth as described in the
510 methods. In addition, a theoretical exponential decay curve with depth is generated to
511 represent a pH profile that closely tracks dissolved oxygen as elsewhere in the global
512 ocean and where the observed increase at the top of the ODZ is absent. Using equation
513 6, calcium carbonate saturation (Ω) is determined for each pH profile. In both cases, the
514 aragonite saturation horizon (Ω = 1) is found above the ODZ, whereas the calcite
515 saturation horizon is found below the ODZ (Figure 9). In addition, differences in Ω
516 between the baseline case with no denitrification and the one where denitrification is
517 permitted is greatest at the local pH maximum as expected, showing denitrification adds
518 buffering capacity in the ocean. The Ω difference between two cases is notably larger
519 for calcite compared to aragonite.

[Figure 9]

520 **4. Discussion**

521 *4.1. High resolution nitrite and pH measurements*

522 Simultaneous measurements of inorganic nitrogen and carbon offer an
523 integrative approach for resolving which metabolisms shape biogeochemistry in the
524 ETNP ODZ. Our relative contributions terms represent the integrated impact of a
525 reaction, as a water parcel traverses the ODZ instead of an instantaneous reaction rate
526 at a specific location or time that can carry methodological artifacts due to the
527 perturbation of natural microbial communities in incubation experiments. Changes in the
528 total alkalinity, pH, and DIC complement DIN measurements in Δtracer calculations and
529 allow further distinction between key reactions. As a result, the system of equations
530 connecting DIN and DIC measurements with relative reaction rates (Equation 2) can be
531 solved successfully.

532 Moreover, investigating ODZ biogeochemistry requires measurements with the
533 high spatial resolution because the ODZ is not a single well-mixed box and consists of
534 distinct biogeochemical regimes along different layers or isopycnal surfaces. For
535 example, low-resolution CLIVAR and GOSHIP measurements (Figure 5) either blend
536 the SNM and TNM together or underrepresent the nitrite accumulation across the SNM,
537 whereas high-resolution FK180624 data show two distinct coherent nitrite peaks. Due to
538 the global nature of CLIVAR and GOSHIP programs, only very low resolution of DIC

539 and DIN measurements within the ODZs is typically permitted. These programs include
540 only a few ODZ stations spanning the entire water column instead of focusing on the
541 suboxic depths. Furthermore, the organic matter composition and size, which is a key
542 factor impacting local relative contributions, vary significantly across the ETNP and with
543 depth (Cram et al., 2022), and could alter the observed individual tracer profiles.
544 Therefore, integrative approaches coupled with high-resolution data such as reaction
545 relative contributions and high-resolution DIC and DIN measurements create a new
546 standard for future investigations of ODZ biogeochemistry.

547 *4.2. Nitrite cycle in the ETNP ODZ*

548 Using simultaneous DIN and DIC measurements, our study determined the
549 composition of the organic matter sinking to the ODZ from the surface. The N:P ratio
550 estimated for the organic matter sinking in the ETNP (11.4:1) is less than the canonical
551 Redfield ratio (16:1) (Anderson, 1995; Redfield, 1958). The N:P ratio observed in the
552 oxycline in the ETNP is considerably less than the Redfield N:P ratio because the fixed
553 nitrogen in the water masses transiting the ODZ is consumed relative to phosphate via
554 denitrification and anammox. These water masses upwell in the coastal areas of the
555 ODZ to supply the surface ocean with similarly depleted fixed nitrogen and a low N:P
556 ratio. We continue to find anammox is the dominant pathway for nitrogen loss in the
557 ETNP overall regardless of C_{ox} and C:N:P ratio, but the specific magnitude of anammox
558 % depends on C:N:P ratio. Because denitrification, not anammox, produces the
559 climatically important gas N_2O, the dependence of the contribution of denitrification to
560 fixed nitrogen loss on the N-content of organic matter affects N_2O production. This
561 organic matter remineralized in the ODZ can be sourced, in addition to sinking surface
562 material, from marine organisms such as zooplankton migrating into ODZ (Bianchi et
563 al., 2014; Cram et al., 2022). The composition of the zooplankton-derived organic
564 matter is reported to be enriched in nitrogen compared to the canonical stoichiometry
565 (Pitt et al., 2009; Ventura, 2006). The resulting lower C:N ratio would yield an increased
566 anammox %, as suggested by Figures 7a and 7d in order to consume additional
567 ammonium produced by DNRN and denitrification. Reconciliating the organic matter
568 supply to ODZs remains a long-standing need.

569 Denitrification relative contribution values imply that denitrification is within one
570 order of magnitude of anammox, similar to other studies in the Pacific ODZs (Babbin,
571 Buchwald, et al., 2020; Babbin et al., 2017; Peng et al., 2015). Other studies report that
572 anammox, while affected, is less inhibited by oxygen than denitrification (Dalsgaard et
573 al., 2014), which explains higher anammox relative contribution values at the anoxic-
574 oxic interface (top and bottom 3 layers) in Figure 6. Calculated anammox % strongly
575 depends on C_{ox} at the top of the ODZ, implying that denitrification is enhanced by higher
576 carbon oxidation states when the environment is fully anoxic. The standard deviation in
577 the relative contributions (Figure 6) is generated by the error in Δtracer best-fits for each
578 layer. These standard deviation values also suggest that the total reduction of nitrite is
579 better constrained than the partitioning between anammox and denitrification, potentially
580 explaining why there is less agreement between previous studies regarding anammox
581 % in the ODZs. Additionally, denitrification in anaerobic particles outside and within the
582 anoxic core (Bianchi et al., 2018; Fuchsman, Paul, et al., 2019) could alter the relative
583 contributions. Here, denitrification in particles is not distinguished from the water column
584 as we solely ascertain integrated metabolic impacts on the water. Additionally,
585 denitrification outside of the 16 layers is not investigated as the simple system of
586 reactions (Table 2) does not capture the biogeochemistry outside the anoxic core and
587 suboxic boundaries.
588 Even though our work does not directly determine changes in nitrite oxidation
589 rate magnitudes with depth, the shape of nitrite oxidation relative contribution with
590 respect to nitrite reduction and DNRN is consistent with studies in the ETSP and ETNP
591 ODZ cores in which nitrite oxidation is more important at the edges of the ODZ (Babbin,
592 Buchwald, et al., 2020; Peng et al., 2015, 2016). Furthermore, nitrite oxidation to
593 reduction ratios are expected between 0-6.5 and nitrite oxidation to DNRN ratios are
594 between 0-0.8 in the ETSP ODZ from integrated natural abundance isotope surveys
595 (Casciotti et al., 2013). The ratios calculated by our novel relative reaction contribution
596 method fall within these ranges at the top of the ODZ and the TNM. Furthermore, the
597 highest denitrification rates are likely to be observed at the ODZ top compared to the
598 rest of the ODZ core (Babbin, Buchwald, et al., 2020). The low nitrite oxidation to
599 reduction ratio also suggests that the ODZ top is more significant for fixed nitrogen loss

600 in the ODZ compared to other layers. Recent studies report that the largest N_2
601 concentrations are found deeper within the ODZ (Fuchsman et al., 2018). The
602 difference could be attributed to physical aspects such as the residence time of water
603 masses and their chemical constituents or to a greater role in migrating zooplankton
604 (Fuchsman et al., 2018), but it requires further investigation. Enhanced denitrification at
605 the top is responsible for low nitrite concentrations in layers 3-4 due to increased nitrite
606 consumption in these layers. Layers at the bottom of the ODZ and in the LNM show
607 amplified nitrite oxidation suggesting a different water column chemistry than that of the
608 anoxic core.

609 Moreover, a comparison between different biogeochemical regimes within the
610 ODZ core (Figure 6) suggests that the SNM and TNM are distinct due to mainly the
611 difference in anammox %. While the SNM has a higher anammox % and nitrite
612 oxidation to reduction ratio, the TNM has a lower anammox % and nitrite oxidation to
613 reduction ratio. Higher nitrite oxidation at the SNM is likely the cause of a decrease in
614 nitrite concentration below the SNM, similar to the ecosystem oscillation trend in the
615 ODZ core investigated by Penn et al., (2019) (see their Figure 3A). Furthermore, Penn
616 et al., (2019) reported that physical oxygen supply at low nitrite and ammonium
617 concentrations could induce an increase in nitrite by reestablishing the competitive
618 advantage of aerobic organisms. Even though no detectable oxygen in the anoxic core
619 is observed in the selected FK180624 stations at the time of sampling, physical
620 intrusion of oxygenated water masses is observed in similar regions of the ETNP such
621 as station 1 from AT37-12 cruise (Figure S1c) and as reported by previously (Kwiecinski
622 & Babbin, 2021; Margolskee et al., 2019). Therefore, intrusions of oxygen at nanomolar
623 concentrations might be a likely cause for the nitrite increase above the TNM.

624 *4.3. Denitrification, pH, and calcium carbonate dissolution in the water column*

625 As illustrated in Figures 2-4, the pH peak at the top of the ODZ is coincident with
626 SNM for the majority of stations. According to balanced reactions in Table 1,
627 denitrification and calcium carbonate dissolution increase pH while the other reactions
628 decrease pH, when accounting for both proton consumption and DIC speciation due to
629 CO_2 release. DNRN also consumes protons; however, speciation of the DIC produced
630 more than compensates for this pH increase. Since pH is increasing with depth at the

631 top of ODZ, where denitrification and carbonate saturation are higher, it is likely that this
632 locally higher pH arises due to denitrification rather than calcium carbonate dissolution
633 affecting local chemistry. Indeed, predictions based on the reaction stoichiometries are
634 also verified by the ΔpH calculations performed for denitrification in the ODZ. In
635 addition, Figure 8 implies that nitrogen loss due to denitrification is responsible for the
636 pH increase at the top of the ODZ, even at varying possible carbon oxidation states.
637 Under the observed average temperature, salinity, alkalinity, and phosphate
638 profiles in the ODZ, ambient Ω of aragonite reaches saturation above the ODZ top,
639 while that of calcite reaches saturation below the ODZ. However, metabolic processes
640 such as organic matter remineralization or DNRN above the ODZ and on particles are
641 likely to decrease local pH, and lower Ω further. For instance, the impact of local
642 metabolism on Ω is reported to shift the saturation horizon for calcite to shallower
643 depths that coincide closely with the ambient aragonite saturation horizon (Subhas et
644 al., 2022). Further work into sinking organic matter and calcium carbonate chemistry at
645 highly localized microscales is necessary to elucidate whether the denitrification-driven
646 pH increase helps to preserve $CaCO_3$ and impact biogeochemistry and export.
647
648 **5. Conclusion**
649 High-resolution sampling in the top 1 km of the ETNP ODZ and high-precision
650 measurements of nutrients, total alkalinity, and pH allowed for an investigation of
651 biogeochemical features unique to ODZs. To explain the coincident pH and secondary
652 nitrite maxima as well as the two-peaked structure of nitrite profiles in the anoxic core,
653 we divided the ODZ into 16-layers and determined the spatial distribution of various
654 nitrogen-cycle reactions and calcium carbonate dissolution in each layer. The results
655 suggest that the SNM and TNM are two distinct features derived from variations in the
656 contributions of anammox vis-à-vis denitrification and the ratio of nitrite oxidation to its
657 reduction. Since these distinct features were clearly observed and subsequently
658 analyzed due to high-resolution sampling, future studies investigating the nitrogen cycle
659 in the ODZs need to increase sampling frequency to better understand DIN dynamics in
660 these regions. In addition, the correspondence between the relative contribution of
661 nitrite oxidation and oxygen profiles from AT37-12 imply that the intrusion of oxygenated

662 water masses is a potential source of the LNM and subsequent TNM. However, this
663 study did not examine the role of other potential oxidants such as iodate, iron, or
664 manganese, the in-situ oxygen production by cyanobacteria, or other particle-
665 associated processes such as sulfate reduction or methanogenesis. Furthermore, the
666 pH increase at the ODZ top is attributed to the denitrification reaction considering
667 increased denitrification relative rates at the ODZ top and net consumption of protons by
668 the reaction. The pH increase implies that the dissolution of sinking calcium carbonate
669 particles could be partially abated in the ODZ.

670 **Acknowledgments**

671 We are indebted to the captain and crew of the *R/V Falkor* and *R/V Atlantis* for
672 their assistance at sea. We also thank the chief scientist Stefan Sievert on the AT37-12
673 cruise for enabling CTD sampling. We acknowledge the decades of scientists, marine
674 technicians, ships' crew, and engineers who contributed to CLIVAR and GO-SHIP P18
675 cruises, and NOAA CoastWatch and OceanWatch for providing satellite altimetry data
676 presented in the supplemental information. The *R/V Falkor* ship time was provided by a
677 Schmidt Ocean Institute grant to KLC and ARB. The AT37-12 research cruise was
678 funded by the NSF OCE-1559042 grant. This work was funded by Simons Foundation
679 grant #622065, NSF grants OCE-2138890 and OCE-2142998 to ARB, NSF grants
680 OCE-1923312 and OCE-2148468 to RJW, the MIT Ally of Nature Award, and the
681 generous support of Dr. Bruce L. Heflinger. Additionally, DD was partially funded by an
682 NSF Graduate Research Fellowship. Finally, we thank Babbin lab members and Adam
683 Subhas for their support and comments on the manuscript and Rémi Buisson for his
684 assistance in creating Figure 1.

685

686 **Data Availability**

687 Bottle data from the FK180624 cruise is available through BCO-DMO (https://www.bco-
688 dmo.org/dataset/832389), and CTD (Sea-bird SBE-911+) data is available through
689 Rolling Deck to Repository (https://doi.org/10.7284/129668). CTD data from AT32-12 is
690 available through BCO-DMO (https://www.bco-dmo.org/dataset/739098), and bottle

691 data from AT37-12 is included as a supplement. GO-SHIP and CLIVAR P18 data are
692 available from the GLODAP version 2 database, cruise numbers 33RO20161119 and
693 33RO20071215, respectively. The scripts used in analyzing FK180624 data, developing
694 models in the study, and plotting important figures are available at
695 https://github.com/tcinay/bablab_FK180624.git

References

Adkins, J. F., Naviaux, J. D., Subhas, A. V., Dong, S., & Berelson, W. M. (2021). The Dissolution Rate of CaCO3 in the Ocean. *Annual Review of Marine Science*, *13*(1), 57–80. https://doi.org/10.1146/annurev-marine-041720-092514

Anderson, L. A. (1995). On the hydrogen and oxygen content of marine phytoplankton. *Deep Sea Research Part I: Oceanographic Research Papers*, *42*(9), 1675–1680. https://doi.org/10.1016/0967-0637(95)00072-E

Babbin, A. R., & Ward, B. B. (2013). Controls on Nitrogen Loss Processes in Chesapeake Bay Sediments. *Environmental Science & Technology*, *47*(9), 4189–4196. https://doi.org/10.1021/es304842r

Babbin, A. R., Keil, R. G., Devol, A. H., & Ward, B. B. (2014). Organic Matter Stoichiometry, Flux, and Oxygen Control Nitrogen Loss in the Ocean. *Science*, *344*(6182), 406–408. https://doi.org/10.1126/science.1248364

Babbin, A. R., Bianchi, D., Jayakumar, A., & Ward, B. B. (2015). Rapid nitrous oxide cycling in the suboxic ocean. *Science*, *348*(6239), 1127–1129. https://doi.org/10.1126/science.aaa8380

Babbin, A. R., Peters, B. D., Mordy, C. W., Widner, B., Casciotti, K. L., & Ward, B. B. (2017). Multiple metabolisms constrain the anaerobic nitrite budget in the Eastern Tropical South Pacific. *Global Biogeochemical Cycles*, *31*(2), 258–271. https://doi.org/10.1002/2016GB005407

Babbin, A. R., Buchwald, C., Morel, F. M. M., Wankel, S. D., & Ward, B. B. (2020). Nitrite oxidation exceeds reduction and fixed nitrogen loss in anoxic Pacific waters. *Marine Chemistry*, *224*, 103814. https://doi.org/10.1016/j.marchem.2020.103814

720 Babbin, A. R., Boles, E. L., Mühle, J., & Weiss, R. F. (2020). On the natural spatio-
721 temporal heterogeneity of South Pacific nitrous oxide. *Nature Communications*,
722 *11*(1), 3672. https://doi.org/10.1038/s41467-020-17509-6
723 Bianchi, D., Babbin, A. R., & Galbraith, E. D. (2014). Enhancement of anammox by the
724 excretion of diel vertical migrators. *Proceedings of the National Academy of*
725 *Sciences*, *111*(44), 15653–15658. https://doi.org/10.1073/pnas.1410790111
726 Bianchi, D., Weber, T. S., Kiko, R., & Deutsch, C. (2018). Global niche of marine
727 anaerobic metabolisms expanded by particle microenvironments. *Nature*
728 *Geoscience*, *11*(4), 263–268. https://doi.org/10.1038/s41561-018-0081-0
729 Braman, R. S., & Hendrix, S. A. (1989). Nanogram nitrite and nitrate determination in
730 environmental and biological materials by vanadium(III) reduction with
731 chemiluminescence detection. *Analytical Chemistry*, *61*(24), 2715–2718.
732 https://doi.org/10.1021/ac00199a007
733 Brandes, J. A., & Devol, A. H. (2002). A global marine-fixed nitrogen isotopic budget:
734 Implications for Holocene nitrogen cycling. *Global Biogeochemical Cycles*, *16*(4),
735 67-1-67–14. https://doi.org/10.1029/2001GB001856
736 Brandhorst, W. (1959). Nitrification and Denitrification in the Eastern Tropical North
737 Pacific. *ICES Journal of Marine Science*, *25*(1), 3–20.
738 https://doi.org/10.1093/icesjms/25.1.3
739 Bristow, L. A., Dalsgaard, T., Tiano, L., Mills, D. B., Bertagnolli, A. D., Wright, J. J., et al.
740 (2016). Ammonium and nitrite oxidation at nanomolar oxygen concentrations in
741 oxygen minimum zone waters. *Proceedings of the National Academy of*
742 *Sciences*, *113*(38), 10601–10606. https://doi.org/10.1073/pnas.1600359113

743 Brunner, B., Contreras, S., Lehmann, M. F., Matantseva, O., Rollog, M., Kalvelage, T.,
744 et al. (2013). Nitrogen isotope effects induced by anammox bacteria.
745 *Proceedings of the National Academy of Sciences*, *110*(47), 18994–18999.
746 https://doi.org/10.1073/pnas.1310488110
747 Buchwald, C., & Casciotti, K. L. (2013). Isotopic ratios of nitrite as tracers of the sources
748 and age of oceanic nitrite. *Nature Geoscience*, *6*(4), 308–313.
749 https://doi.org/10.1038/ngeo1745
750 Buchwald, C., Santoro, A. E., Stanley, R. H. R., & Casciotti, K. L. (2015). Nitrogen
751 cycling in the secondary nitrite maximum of the eastern tropical North Pacific off
752 Costa Rica. *Global Biogeochemical Cycles*, *29*(12), 2061–2081.
753 https://doi.org/10.1002/2015GB005187
754 Carter, B. R., Radich, J. A., Doyle, H. L., & Dickson, A. G. (2013). An automated system
755 for spectrophotometric seawater pH measurements. *Limnology and*
756 *Oceanography: Methods*, *11*(1), 16–27. https://doi.org/10.4319/lom.2013.11.16
757 Casciotti, K. L., Buchwald, C., & McIlvin, M. (2013). Implications of nitrate and nitrite
758 isotopic measurements for the mechanisms of nitrogen cycling in the Peru
759 oxygen deficient zone. *Deep Sea Research Part I: Oceanographic Research*
760 *Papers*, *80*, 78–93. https://doi.org/10.1016/j.dsr.2013.05.017
761 Chang, B. X., Devol, A. H., & Emerson, S. R. (2012). Fixed nitrogen loss from the
762 eastern tropical North Pacific and Arabian Sea oxygen deficient zones
763 determined from measurements of N2:Ar. *Global Biogeochemical Cycles*, *26*(3).
764 https://doi.org/10.1029/2011GB004207

765 Chang, B. X., Rich, J. R., Jayakumar, A., Naik, H., Pratihary, A. K., Keil, R. G., et al.
766 (2014). The effect of organic carbon on fixed nitrogen loss in the eastern tropical
767 South Pacific and Arabian Sea oxygen deficient zones. *Limnology and*
768 *Oceanography*, *59*(4), 1267–1274. https://doi.org/10.4319/lo.2014.59.4.1267
769 Codispoti, L. A., Brandes, J. A., Christensen, J. P., Devol, A. H., Naqvi, S. W. A., Paerl,
770 H. W., & Yoshinari, T. (2001). The oceanic fixed nitrogen and nitrous oxide
771 budgets: Moving targets as we enter the anthropocene? *Scientia Marina*, *65*(S2),
772 85–105. https://doi.org/10.3989/scimar.2001.65s285
773 Cram, J. A., Fuchsman, C. A., Duffy, M. E., Pretty, J. L., Lekanoff, R. M., Neibauer, J.
774 A., et al. (2022). Slow Particle Remineralization, Rather Than Suppressed
775 Disaggregation, Drives Efficient Flux Transfer Through the Eastern Tropical
776 North Pacific Oxygen Deficient Zone. *Global Biogeochemical Cycles*, *36*(1),
777 e2021GB007080. https://doi.org/10.1029/2021GB007080
778 Dalsgaard, T., Thamdrup, B., Farías, L., & Revsbech, N. P. (2012). Anammox and
779 denitrification in the oxygen minimum zone of the eastern South Pacific.
780 *Limnology and Oceanography*, *57*(5), 1331–1346.
781 https://doi.org/10.4319/lo.2012.57.5.1331
782 Dalsgaard, T., Stewart, F. J., Thamdrup, B., De Brabandere, L., Revsbech, N. P., Ulloa,
783 O., et al. (2014). Oxygen at Nanomolar Levels Reversibly Suppresses Process
784 Rates and Gene Expression in Anammox and Denitrification in the Oxygen
785 Minimum Zone off Northern Chile. *MBio*, *5*(6), e01966-14.
786 https://doi.org/10.1128/mBio.01966-14

787 D'Errico, J. (2022). inpaint_nans. MATLAB Central File Exchange. Retrieved from
788 (https://www.mathworks.com/matlabcentral/fileexchange/4551-inpaint_nans)
789 Deutsch, C., Gruber, N., Key, R. M., Sarmiento, J. L., & Ganachaud, A. (2001).
790 Denitrification and N2 fixation in the Pacific Ocean. *Global Biogeochemical*
791 *Cycles*, *15*(2), 483–506. https://doi.org/10.1029/2000GB001291
792 Devol, A. H. (2003). Solution to a marine mystery. *Nature*, *422*(6932), 575–576.
793 https://doi.org/10.1038/422575a
794 DeVries, T., Deutsch, C., Rafter, P. A., & Primeau, F. (2013). Marine denitrification rates
795 determined from a global 3-D inverse model. *Biogeosciences*, *10*(4), 2481–2496.
796 https://doi.org/10.5194/bg-10-2481-2013
797 Dickson, A. G., Sabine, C. L., & Christian, J. R. (2007). *Guide to Best Practices for*
798 *Ocean CO2 Measurements.* (Report). North Pacific Marine Science
799 Organization. Retrieved from
800 https://repository.oceanbestpractices.org/handle/11329/249
801 Evans, N., Boles, E., Kwiecinski, J. V., Mullen, S., Wolf, M., Devol, A. H., et al. (2020).
802 The role of water masses in shaping the distribution of redox active compounds
803 in the Eastern Tropical North Pacific oxygen deficient zone and influencing low
804 oxygen concentrations in the eastern Pacific Ocean. *Limnology and*
805 *Oceanography*, *65*(8), 1688–1705. https://doi.org/10.1002/lno.11412
806 Feely, R. A., Sabine, C. L., Lee, K., Millero, F. J., Lamb, M. F., Greeley, D., et al. (2002).
807 In situ calcium carbonate dissolution in the Pacific Ocean. *Global*
808 *Biogeochemical Cycles*, *16*(4), 91-1-91–12.
809 https://doi.org/10.1029/2002GB001866

Firing, E., Filipe, Barna, A., & Abernathey, R. (2021, August). TEOS-10/GSW-Python: v3.4.1.post0 (Version v3.4.1.post0). Zenodo. https://doi.org/10.5281/zenodo.5214122

Fuchsman, C. A., Devol, A. H., Saunders, J. K., McKay, C., & Rocap, G. (2017). Niche Partitioning of the N Cycling Microbial Community of an Offshore Oxygen Deficient Zone. *Frontiers in Microbiology*, *8*. Retrieved from https://www.frontiersin.org/articles/10.3389/fmicb.2017.02384

Fuchsman, C. A., Devol, A. H., Casciotti, K. L., Buchwald, C., Chang, B. X., & Horak, R. E. A. (2018). An N isotopic mass balance of the Eastern Tropical North Pacific oxygen deficient zone. *Deep Sea Research Part II: Topical Studies in Oceanography*, *156*, 137–147. https://doi.org/10.1016/j.dsr2.2017.12.013

Fuchsman, C. A., Palevsky, H. I., Widner, B., Duffy, M., Carlson, M. C. G., Neibauer, J. A., et al. (2019). Cyanobacteria and cyanophage contributions to carbon and nitrogen cycling in an oligotrophic oxygen-deficient zone. *The ISME Journal*, *13*(11), 2714–2726. https://doi.org/10.1038/s41396-019-0452-6

Fuchsman, C. A., Paul, B., Staley, J. T., Yakushev, E. V., & Murray, J. W. (2019). Detection of Transient Denitrification During a High Organic Matter Event in the Black Sea. *Global Biogeochemical Cycles*, *33*(2), 143–162. https://doi.org/10.1029/2018GB006032

Füssel, J., Lam, P., Lavik, G., Jensen, M. M., Holtappels, M., Günter, M., & Kuypers, M. M. (2012). Nitrite oxidation in the Namibian oxygen minimum zone. *The ISME Journal*, *6*(6), 1200–1209. https://doi.org/10.1038/ismej.2011.178

832 Ganesh, S., Bristow, L. A., Larsen, M., Sarode, N., Thamdrup, B., & Stewart, F. J.
833 (2015). Size-fraction partitioning of community gene transcription and nitrogen
834 metabolism in a marine oxygen minimum zone. *The ISME Journal*, *9*(12), 2682–
835 2696. https://doi.org/10.1038/ismej.2015.44
836 Garcia-Robledo, E., Padilla, C. C., Aldunate, M., Stewart, F. J., Ulloa, O., Paulmier, A.,
837 et al. (2017). Cryptic oxygen cycling in anoxic marine zones. *Proceedings of the*
838 *National Academy of Sciences*, *114*(31), 8319–8324.
839 https://doi.org/10.1073/pnas.1619844114
840 Gruber, N., & Sarmiento, J. L. (1997). Global patterns of marine nitrogen fixation and
841 denitrification. *Global Biogeochemical Cycles*, *11*(2), 235–266.
842 https://doi.org/10.1029/97GB00077
843 Hardisty, D. S., Horner, T. J., Evans, N., Moriyasu, R., Babbin, A. R., Wankel, S. D., et
844 al. (2021). Limited iodate reduction in shipboard seawater incubations from the
845 Eastern Tropical North Pacific oxygen deficient zone. *Earth and Planetary*
846 *Science Letters*, *554*, 116676. https://doi.org/10.1016/j.epsl.2020.116676
847 Hernandez-Ayon, J. M., Paulmier, A., Garcon, V., Sudre, J., Montes, I., Chapa-Balcorta,
848 C., et al. (2019). Dynamics of the Carbonate System Across the Peruvian
849 Oxygen Minimum Zone. *Frontiers in Marine Science*, *6*, 617.
850 https://doi.org/10.3389/fmars.2019.00617
851 Huber, P. J. (1973). Robust Regression: Asymptotics, Conjectures and Monte Carlo.
852 *The Annals of Statistics*, *1*(5), 799–821.
853 Humphreys, M., Pierrot, D., & van Heuven, S. (2020). PyCO2SYS: marine carbonate
854 system calculations in Python. *Version 1.3. 0. Zenodo*.

855 Ji, Q., Babbin, A. R., Jayakumar, A., Oleynik, S., & Ward, B. B. (2015). Nitrous oxide
856 production by nitrification and denitrification in the Eastern Tropical South Pacific
857 oxygen minimum zone. *Geophysical Research Letters*, *42*(24), 10,755-10,764.
858 https://doi.org/10.1002/2015GL066853
859 Jiang, L.-Q., Carter, B. R., Feely, R. A., Lauvset, S. K., & Olsen, A. (2019). Surface
860 ocean pH and buffer capacity: past, present and future. *Scientific Reports*, *9*(1),
861 18624. https://doi.org/10.1038/s41598-019-55039-4
862 Jørgensen, B. B. (1982). Mineralization of organic matter in the sea bed—the role of
863 sulphate reduction. *Nature*, *296*(5858), 643–645.
864 https://doi.org/10.1038/296643a0
865 Kalvelage, T., Lavik, G., Lam, P., Contreras, S., Arteaga, L., Löscher, C. R., et al.
866 (2013). Nitrogen cycling driven by organic matter export in the South Pacific
867 oxygen minimum zone. *Nature Geoscience*, *6*(3), 228–234.
868 https://doi.org/10.1038/ngeo1739
869 Karstensen, J., Stramma, L., & Visbeck, M. (2008). Oxygen minimum zones in the
870 eastern tropical Atlantic and Pacific oceans. *Progress in Oceanography*, *77*(4),
871 331–350. https://doi.org/10.1016/j.pocean.2007.05.009
872 Koeve, W., & Kähler, P. (2010). Heterotrophic denitrification vs. autotrophic anammox –
873 quantifying collateral effects on the oceanic carbon cycle. *Biogeosciences*, *7*(8),
874 2327–2337. https://doi.org/10.5194/bg-7-2327-2010
875 Kwiecinski, J. V., & Babbin, A. R. (2021). A High-Resolution Atlas of the Eastern
876 Tropical Pacific Oxygen Deficient Zones. *Global Biogeochemical Cycles*, *35*(12),
877 e2021GB007001. https://doi.org/10.1029/2021GB007001

878 Lam, P., Lavik, G., Jensen, M. M., Vossenberg, J. van de, Schmid, M., Woebken, D., et
879 al. (2009). Revising the nitrogen cycle in the Peruvian oxygen minimum zone.
880 *Proceedings of the National Academy of Sciences*, *106*(12), 4752–4757.
881 https://doi.org/10.1073/pnas.0812444106
882 Lauvset, S. K., Lange, N., Tanhua, T., Bittig, H. C., Olsen, A., Kozyr, A., et al. (2021).
883 An updated version of the global interior ocean biogeochemical data product,
884 GLODAPv2.2021. *Earth System Science Data*, *13*(12), 5565–5589.
885 https://doi.org/10.5194/essd-13-5565-2021
886 Lee, K., Kim, T.-W., Byrne, R. H., Millero, F. J., Feely, R. A., & Liu, Y.-M. (2010). The
887 universal ratio of boron to chlorinity for the North Pacific and North Atlantic
888 oceans. *Geochimica et Cosmochimica Acta*, *74*(6), 1801–1811.
889 https://doi.org/10.1016/j.gca.2009.12.027
890 Lipschultz, F., Zafiriou, O. C., & Ball, L. A. (1996). Seasonal fluctuations of nitrite
891 concentrations in the deep oligotrophic ocean. *Deep Sea Research Part II:*
892 *Topical Studies in Oceanography*, *43*(2), 403–419. https://doi.org/10.1016/0967-
893 0645(96)00003-3
894 Lomas, M. W., & Lipschultz, F. (2006). Forming the primary nitrite maximum: Nitrifiers or
895 phytoplankton? *Limnology and Oceanography*, *51*(5), 2453–2467.
896 https://doi.org/10.4319/lo.2006.51.5.2453
897 López-Sandoval, D. C., Lara-Lara, J. R., Lavín, M. F., Álvarez-Borrego, S., & Gaxiola-
898 Castro, G. (2009). Primary productivity observations in the eastern tropical
899 Pacific off Cabo Corrientes, Mexico. *Ciencias Marinas*, *35*(2), 169–182.
900 https://doi.org/10.7773/cm.v35i2.1530

Lueker, T. J., Dickson, A. G., & Keeling, C. D. (2000). Ocean pCO2 calculated from dissolved inorganic carbon, alkalinity, and equations for K1 and K2: validation based on laboratory measurements of CO2 in gas and seawater at equilibrium. *Marine Chemistry*, *70*(1), 105–119. https://doi.org/10.1016/S0304-4203(00)00022-0

Margolskee, A., Frenzel, H., Emerson, S., & Deutsch, C. (2019). Ventilation Pathways for the North Pacific Oxygen Deficient Zone. *Global Biogeochemical Cycles*, *33*(7), 875–890. https://doi.org/10.1029/2018GB006149

Millero, F. J. (2007). The Marine Inorganic Carbon Cycle. *Chemical Reviews*, *107*(2), 308–341. https://doi.org/10.1021/cr0503557

Milliman, J. D., Troy, P. J., Balch, W. M., Adams, A. K., Li, Y.-H., & Mackenzie, F. T. (1999). Biologically mediated dissolution of calcium carbonate above the chemical lysocline? *Deep Sea Research Part I: Oceanographic Research Papers*, *46*(10), 1653–1669. https://doi.org/10.1016/S0967-0637(99)00034-5

Moreno, A. R., Garcia, C. A., Larkin, A. A., Lee, J. A., Wang, W.-L., Moore, J. K., et al. (2020). Latitudinal gradient in the respiration quotient and the implications for ocean oxygen availability. *Proceedings of the National Academy of Sciences*, *117*(37), 22866–22872. https://doi.org/10.1073/pnas.2004986117

Moriyasu, R., Evans, N., Bolster, K. M., Hardisty, D. S., & Moffett, J. W. (2020). The Distribution and Redox Speciation of Iodine in the Eastern Tropical North Pacific Ocean. *Global Biogeochemical Cycles*, *34*(2), e2019GB006302. https://doi.org/10.1029/2019GB006302

923 Morrison, J. M., Codispoti, L. A., Gaurin, S., Jones, B., Manghnani, V., & Zheng, Z.
924 (1998). Seasonal variation of hydrographic and nutrient fields during the US
925 JGOFS Arabian Sea Process Study. *Deep Sea Research Part II: Topical Studies*
926 *in Oceanography*, *45*(10), 2053–2101. https://doi.org/10.1016/S0967-
927 0645(98)00063-0
928 Naqvi, S. W. A., Jayakumar, D. A., Narvekar, P. V., Naik, H., Sarma, V. V. S. S.,
929 D'Souza, W., et al. (2000). Increased marine production of N2O due to
930 intensifying anoxia on the Indian continental shelf. *Nature*, *408*(6810), 346–349.
931 https://doi.org/10.1038/35042551
932 Olsen, A., Lange, N., Key, R. M., Tanhua, T., Álvarez, M., Becker, S., et al. (2019).
933 GLODAPv2.2019 – an update of GLODAPv2. *Earth System Science Data*, *11*(3),
934 1437–1461. https://doi.org/10.5194/essd-11-1437-2019
935 Olsen, A., Lange, N., Key, R. M., Tanhua, T., Bittig, H. C., Kozyr, A., et al. (2020). An
936 updated version of the global interior ocean biogeochemical data product,
937 GLODAPv2.2020. *Earth System Science Data*, *12*(4), 3653–3678.
938 https://doi.org/10.5194/essd-12-3653-2020
939 Pan, Y., Li, Y., Ma, Q., He, H., Wang, S., Sun, Z., et al. (2021). The role of Mg2+ in
940 inhibiting CaCO3 precipitation from seawater. *Marine Chemistry*, *237*, 104036.
941 https://doi.org/10.1016/j.marchem.2021.104036
942 Paulmier, A., & Ruiz-Pino, D. (2009). Oxygen minimum zones (OMZs) in the modern
943 ocean. *Progress in Oceanography*, *80*(3), 113–128.
944 https://doi.org/10.1016/j.pocean.2008.08.001

945 Paulmier, A., Kriest, I., & Oschlies, A. (2009). Stoichiometries of remineralisation and
946 denitrification in global biogeochemical ocean models. *Biogeosciences*, *6*(5),
947 923–935. https://doi.org/10.5194/bg-6-923-2009
948 Paulmier, A., Ruiz-Pino, D., & Garçon, V. (2011). CO_2 maximum in the oxygen minimum
949 zone (OMZ). *Biogeosciences*, *8*(2), 239–252. https://doi.org/10.5194/bg-8-239-
950 2011
951 Pedregosa, F., Varoquaux, G., Gramfort, A., Michel, V., Thirion, B., Grisel, O., et al.
952 (2011). Scikit-learn: Machine Learning in Python. *Journal of Machine Learning*
953 *Research*, *12*, 2825–2830.
954 Peng, X., Fuchsman, C. A., Jayakumar, A., Oleynik, S., Martens-Habbena, W., Devol,
955 A. H., & Ward, B. B. (2015). Ammonia and nitrite oxidation in the Eastern
956 Tropical North Pacific. *Global Biogeochemical Cycles*, *29*(12), 2034–2049.
957 https://doi.org/10.1002/2015GB005278
958 Peng, X., Fuchsman, C. A., Jayakumar, A., Warner, M. J., Devol, A. H., & Ward, B. B.
959 (2016). Revisiting nitrification in the Eastern Tropical South Pacific: A focus on
960 controls. *Journal of Geophysical Research: Oceans*, *121*(3), 1667–1684.
961 https://doi.org/10.1002/2015JC011455
962 Penn, J. L., Weber, T., Chang, B. X., & Deutsch, C. (2019). Microbial ecosystem
963 dynamics drive fluctuating nitrogen loss in marine anoxic zones. *Proceedings of*
964 *the National Academy of Sciences*, *116*(15), 7220–7225.
965 https://doi.org/10.1073/pnas.1818014116
966 Pennington, J. T., Mahoney, K. L., Kuwahara, V. S., Kolber, D. D., Calienes, R., &
967 Chavez, F. P. (2006). Primary production in the eastern tropical Pacific: A review.

Progress in Oceanography, *69*(2), 285–317. https://doi.org/10.1016/j.pocean.2006.03.012

Perez, F. F., & Fraga, F. (1987). Association constant of fluoride and hydrogen ions in seawater. *Marine Chemistry*, *21*(2), 161–168. https://doi.org/10.1016/0304-4203(87)90036-3

Peters, B. D., Babbin, A. R., Lettmann, K. A., Mordy, C. W., Ulloa, O., Ward, B. B., & Casciotti, K. L. (2016). Vertical modeling of the nitrogen cycle in the eastern tropical South Pacific oxygen deficient zone using high-resolution concentration and isotope measurements. *Global Biogeochemical Cycles*, *30*(11), 1661–1681. https://doi.org/10.1002/2016GB005415

Pitt, K. A., Welsh, D. T., & Condon, R. H. (2009). Influence of jellyfish blooms on carbon, nitrogen and phosphorus cycling and plankton production. *Hydrobiologia*, *616*(1), 133–149. https://doi.org/10.1007/s10750-008-9584-9

Raven, M. R., Keil, R. G., & Webb, S. M. (2021). Microbial sulfate reduction and organic sulfur formation in sinking marine particles. *Science*, *371*(6525), 178–181. https://doi.org/10.1126/science.abc6035

Ravishankara, A., Daniel, J. S., & Portmann, R. W. (2009). Nitrous oxide (N2O): the dominant ozone-depleting substance emitted in the 21st century. *Science*, *326*(5949), 123–125.

Redfield, A. C. (1958). The biological control of chemical factors in the environment. *American Scientist*, *46*(3), 230A–221.

Revsbech, N. P., Larsen, L. H., Gundersen, J., Dalsgaard, T., Ulloa, O., & Thamdrup, B. (2009). Determination of ultra-low oxygen concentrations in oxygen minimum

991 zones by the STOX sensor. *Limnology and Oceanography: Methods*, *7*(5), 371–
992 381. https://doi.org/10.4319/lom.2009.7.371
993 Sasakawa, M., Tsunogai, U., Kameyama, S., Nakagawa, F., Nojiri, Y., & Tsuda, A.
994 (2008). Carbon isotopic characterization for the origin of excess methane in
995 subsurface seawater. *Journal of Geophysical Research: Oceans*, *113*(C3).
996 https://doi.org/10.1029/2007JC004217
997 Saunders, J. K., Fuchsman, C. A., McKay, C., & Rocap, G. (2019). Complete arsenic-
998 based respiratory cycle in the marine microbial communities of pelagic oxygen-
999 deficient zones. *Proceedings of the National Academy of Sciences*, *116*(20),
1000 9925–9930. https://doi.org/10.1073/pnas.1818349116
1001 Schmale, O., Wäge, J., Mohrholz, V., Wasmund, N., Gräwe, U., Rehder, G., et al.
1002 (2018). The contribution of zooplankton to methane supersaturation in the
1003 oxygenated upper waters of the central Baltic Sea. *Limnology and*
1004 *Oceanography*, *63*(1), 412–430. https://doi.org/10.1002/lno.10640
1005 Stramma, L., Schmidtko, S., Levin, L. A., & Johnson, G. C. (2010). Ocean oxygen
1006 minima expansions and their biological impacts. *Deep Sea Research Part I:*
1007 *Oceanographic Research Papers*, *57*(4), 587–595.
1008 https://doi.org/10.1016/j.dsr.2010.01.005
1009 Strickland, J. D. H., & Parsons, T. R. (1972). A practical handbook of seawater analysis.
1010 Strous, M., Heijnen, J. J., Kuenen, J. G., & Jetten, M. S. M. (1998). The sequencing
1011 batch reactor as a powerful tool for the study of slowly growing anaerobic
1012 ammonium-oxidizing microorganisms. *Applied Microbiology and Biotechnology*,
1013 *50*(5), 589–596. https://doi.org/10.1007/s002530051340

1014 Subhas, A. V., Dong, S., Naviaux, J. D., Rollins, N. E., Ziveri, P., Gray, W., et al. (2022).
1015 Shallow Calcium Carbonate Cycling in the North Pacific Ocean. *Global*
1016 *Biogeochemical Cycles*, *36*(5), e2022GB007388.
1017 https://doi.org/10.1029/2022GB007388
1018 Thamdrup, B., Dalsgaard, T., & Revsbech, N. P. (2012). Widespread functional anoxia
1019 in the oxygen minimum zone of the Eastern South Pacific. *Deep Sea Research*
1020 *Part I: Oceanographic Research Papers*, *65*, 36–45.
1021 https://doi.org/10.1016/j.dsr.2012.03.001
1022 Thamdrup, B., Steinsdóttir, H. G. R., Bertagnolli, A. D., Padilla, C. C., Patin, N. V.,
1023 Garcia-Robledo, E., et al. (2019). Anaerobic methane oxidation is an important
1024 sink for methane in the ocean's largest oxygen minimum zone. *Limnology and*
1025 *Oceanography*, *64*(6), 2569–2585. https://doi.org/10.1002/lno.11235
1026 Tiano, L., Garcia-Robledo, E., Dalsgaard, T., Devol, A. H., Ward, B. B., Ulloa, O., et al.
1027 (2014). Oxygen distribution and aerobic respiration in the north and south
1028 eastern tropical Pacific oxygen minimum zones. *Deep Sea Research Part I:*
1029 *Oceanographic Research Papers*, *94*, 173–183.
1030 https://doi.org/10.1016/j.dsr.2014.10.001
1031 Tsementzi, D., Wu, J., Deutsch, S., Nath, S., Rodriguez-R, L. M., Burns, A. S., et al.
1032 (2016). SAR11 bacteria linked to ocean anoxia and nitrogen loss. *Nature*,
1033 *536*(7615), 179–183. https://doi.org/10.1038/nature19068
1034 Van Heuven, S., Pierrot, D., Rae, J., Lewis, E., & Wallace, D. (2011). MATLAB Program
1035 developed for CO2 system calculations, ORNL/CDIAC-105b. *Carbon Dioxide*

Information Analysis Center, Oak Ridge National Laboratory, US Department of Energy, Oak Ridge, Tennessee, *530*.

Ventura, M. (2006). Linking biochemical and elemental composition in freshwater and marine crustacean zooplankton. *Marine Ecology Progress Series*, *327*, 233–246. https://doi.org/10.3354/meps327233

Virtanen, P., Gommers, R., Oliphant, T. E., Haberland, M., Reddy, T., Cournapeau, D., et al. (2020). SciPy 1.0: Fundamental Algorithms for Scientific Computing in Python. *Nature Methods*, *17*, 261–272. https://doi.org/10.1038/s41592-019-0686-2

Ward, B. B. (2013). How nitrogen is lost. *Science*, *341*(6144), 352–353.

Ward, B. B., Devol, A. H., Rich, J. J., Chang, B. X., Bulow, S. E., Naik, H., et al. (2009). Denitrification as the dominant nitrogen loss process in the Arabian Sea. *Nature*, *461*(7260), 78–81. https://doi.org/10.1038/nature08276

Widner, B., Fuchsman, C. A., Chang, B. X., Rocap, G., & Mulholland, M. R. (2018). Utilization of urea and cyanate in waters overlying and within the eastern tropical north Pacific oxygen deficient zone. *FEMS Microbiology Ecology*, *94*(10), fiy138. https://doi.org/10.1093/femsec/fiy138

Woosley, R. J. (2021). Long-term stability and storage of meta-cresol purple solutions for seawater pH measurements. *Limnology and Oceanography: Methods*, *19*(12), 810–817. https://doi.org/10.1002/lom3.10462

Woosley, R. J., Millero, F. J., & Grosell, M. (2012). The solubility of fish-produced high magnesium calcite in seawater. *Journal of Geophysical Research: Oceans*, *117*(C4). https://doi.org/10.1029/2011JC007599

1059 Zakem, E. J., & Follows, M. J. (2017). A theoretical basis for a nanomolar critical
1060 oxygen concentration. *Limnology and Oceanography*, *62*(2), 795–805.
1061 https://doi.org/10.1002/lno.10461
1062 Zakem, E. J., Al-Haj, A., Church, M. J., van Dijken, G. L., Dutkiewicz, S., Foster, S. Q.,
1063 et al. (2018). Ecological control of nitrite in the upper ocean. *Nature*
1064 *Communications*, *9*(1), 1206. https://doi.org/10.1038/s41467-018-03553-w
1065 Zhang, Y., Qin, W., Hou, L., Zakem, E. J., Wan, X., Zhao, Z., et al. (2020). Nitrifier
1066 adaptation to low energy flux controls inventory of reduced nitrogen in the dark
1067 ocean. *Proceedings of the National Academy of Sciences*, *117*(9), 4823–4830.
1068 https://doi.org/10.1073/pnas.1912367117

1069

Figure Captions

Figure 1. Conceptual illustration of the major nitrogen and carbon cycling reactions in the ETNP ODZ. DIN species are colored green, DIC species are colored red, and protons are colored purple. Heterotrophic processes are represented as consuming organic matter and releasing CO_2 and NH_4^+, while autotrophic processes are represented as consuming CO_2 and NH_4^+ and producing organic matter.

Figure 2. (a) Dissolved oxygen concentration at σ_θ = 26.2 kg m^{-3} potential density surface in the Eastern Tropical North Pacific. Gridded O_2 concentration data are from Kwiecinski & Babbin (2021). The area enclosed by dashed lines is plotted separately in panel (b) with the *R/V Falkor* cruise track overlayed on the oxygen concentration contours. Interpreting the dissolved oxygen data is performed using the inpaint_nans() function on MATLAB R2021b (D'Errico, 2022). (c) Oxygen, nitrite, and pH vertical profiles in the ETNP ODZ (25.0 < σ_θ <27.4 kg m^{-3}) for a representative collection of stations. Figure S2 shows the same profiles with depth (dbar) as the y-axis. The background shading indicates 16 layers, starting with layer 1 at the top, defined based on the three profiles. See Table S1 for potential density anomaly and depth ranges for each layer.

Figure 3. Vertical nitrite (a) and pH (b) profiles between σ_θ = 25.4 – 27.0 kg m^{-3} at each station respectively. Color for each station is based on the maximum nitrite concentration and pH values within the σ_θ range. Darker colors denote higher nitrite concentrations and pH values.

Figure 4. Measured tracer profiles at Station 9 during FK180624 research cruise. The accuracy of total alkalinity measurements was 0.11 ± 1.77 µmol kg^{-1}, determined from certified reference material (CRM). The TA precision was ± 2.28 µmol kg^{-1} determined from duplicates (N=46). The precision of pH measurements was ± 0.0025 from (N=58) duplicates. The precision of NO_x^- (NO_2^- + NO_3^-) was ± 0.035 µmol kg^{-1} from (N=39) duplicates. The precision of nitrite (NO_2^-) measurements was ± 0.14 µmol kg^{-1} from (N = 32) duplicates. The precision of ammonium (NH_4^+) measurements was ± 0.056 µmol kg^{-}

1098 ^{1} from (N = 32) duplicates. The precision of dissolved inorganic phosphorus (DIP)
1099 measurements was ± 0.46 μmol kg^{-1} from (N = 32) duplicates. Precision calculations
1100 with duplicates is based on (Dickson et al., 2007).

1101 **Figure 5.** Vertical oxygen, nitrite and pH profiles with respect to potential density
1102 anomaly in the Eastern Tropical North Pacific along the P18 line over a decade.
1103 CLIVAR and GO-SHIP P18 data are obtained from GLODAP v2.2021 (Lauvset et al.,
1104 2021; Olsen et al., 2019, 2020). GO-SHIP and CLIVAR P18 data are from cruises
1105 33RO20161119 and 33RO20071215 respectively. Oxygen concentration data are
1106 shifted to align all the profiles at 0 μmol kg^{-1} in the ODZ core. Therefore, a new
1107 parameter $\tilde{O}_2$ is defined. 0.5, 3.2, and 2.5 μmol kg^{-1} is subtracted for each data point in
1108 FK180624, CLIVAR and GO-SHIP respectively to $\tilde{O}_2$ parameter.

1109 **Figure 6**. Relative contribution of key reactions to nitrogen and carbon chemistry in
1110 each of 16 layers in the ODZ. The results are for the organic matter with +0.99 carbon
1111 oxidation state. Secondary nitrite maximum (SNM), tertiary nitrite maximum (TNM), and
1112 local nitrite minimum (LNM), and ODZ boundaries are indicated with arrows on the right
1113 side. 50% value is marked with a vertical red dashed line. Reference tracer for panels a,
1114 b, c, e is nitrite. Reference tracer for panel d is nitrate. Reference tracer for panel f is
1115 DIC. Equations for calculating each relative contribution value are given in equations 3–
1116 4 and S1–S10.

1117 **Figure 7** (a,d) Anammox % for nitrite reduction to N_2 compared to denitrification, (b,e)
1118 nitrite oxidation to nitrite reduction ratio, and (c,f) nitrite oxidation to DNRN ratio for four
1119 layers in the ETNP ODZ based on relative contribution analysis. Panels a-c are based
1120 on C:N:P ratio (112.5:11.4:1 mol/mol) calculated in this study and panels d-f are based
1121 on Redfield C:N:P ratio (106:16:1 mol/mol). Layers 4, 6, 7, 11, 14 correspond to the top
1122 of the ODZ, secondary nitrite maximum, local nitrite minimum, tertiary nitrite maximum,
1123 and bottom of the ODZ respectively. Gray shading represents the range of carbon
1124 oxidation states ($-1.92 < C_{ox} < -0.32$) reported by Moreno et al (2020) in the ETNP and
1125 the dashed lines represent +0.18 and +0.99.

1126 **Figure 8.** (a) Expected change in pH per organic carbon (C_{ox} = +0.99) remineralized at
1127 the top of ETNP ODZ due to denitrification compared to a baseline case with no
1128 denitrification for a range of TA and DIC values. (b) Expected change in pH per organic
1129 carbon with varying oxidation state due to denitrification. Each data point represents the
1130 mean ΔpH within the red box on panel (a) which corresponds to observed TA and DIC
1131 values in the ODZ. Gray shading represents the range of carbon oxidation states (-1.92
1132 < C_{ox} < -0.32) reported by Moreno et al (2020) in the ETNP and the dashed lines
1133 represents +0.18 and +0.99.

1134 **Figure 9.** (a) pH and (b) aragonite and calcite saturation state depth profiles in the
1135 ETNP. Data collected in the study for the selected stations are represented as blue
1136 dots. Solid lines represent the fit to the data points while the dashed lines represent
1137 hypothetical scenario where no pH increase is observed at the top of the ODZ and there
1138 is no physical water mass mixing at depth.

1139 **Table 1.** Key reactions observed in the ETNP ODZ for the generic organic matter (OM)
1140 composition $C_aH_bO_cN_dP_e$.

1141 **Table 2.** Reaction matrix (R) for the sinking organic matter ($C_{112.5}H_bO_cN_{11.4}P,\ b-2c=$
1142 $-82.17,\ C_{ox}=\ +0.99$). All the values are normalized to ΔDIC for each reaction.
1143

Figure 1.

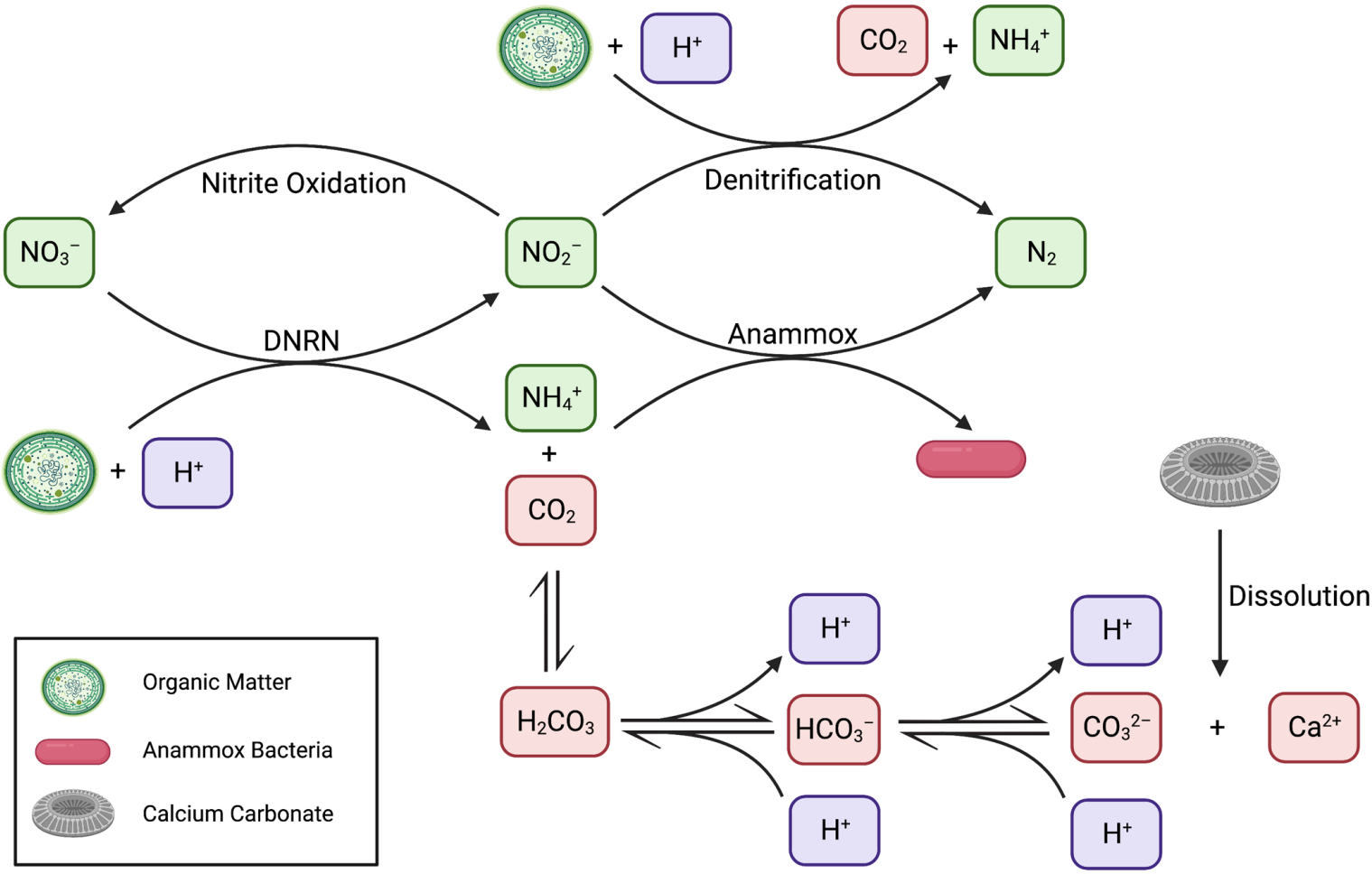
+
H+
CO2
+
NH4+
Nitrite Oxidation
Denitrification
NO3−
NO2−
N2
DNRN
Anammox
NH4+
+
+
H+
CO2
Dissolution
Organic Matter
Anammox Bacteria
Calcium Carbonate
H+
H+
H2CO3
HCO3−
CO32−
+
Ca2+
H+
H+

Figure 2.

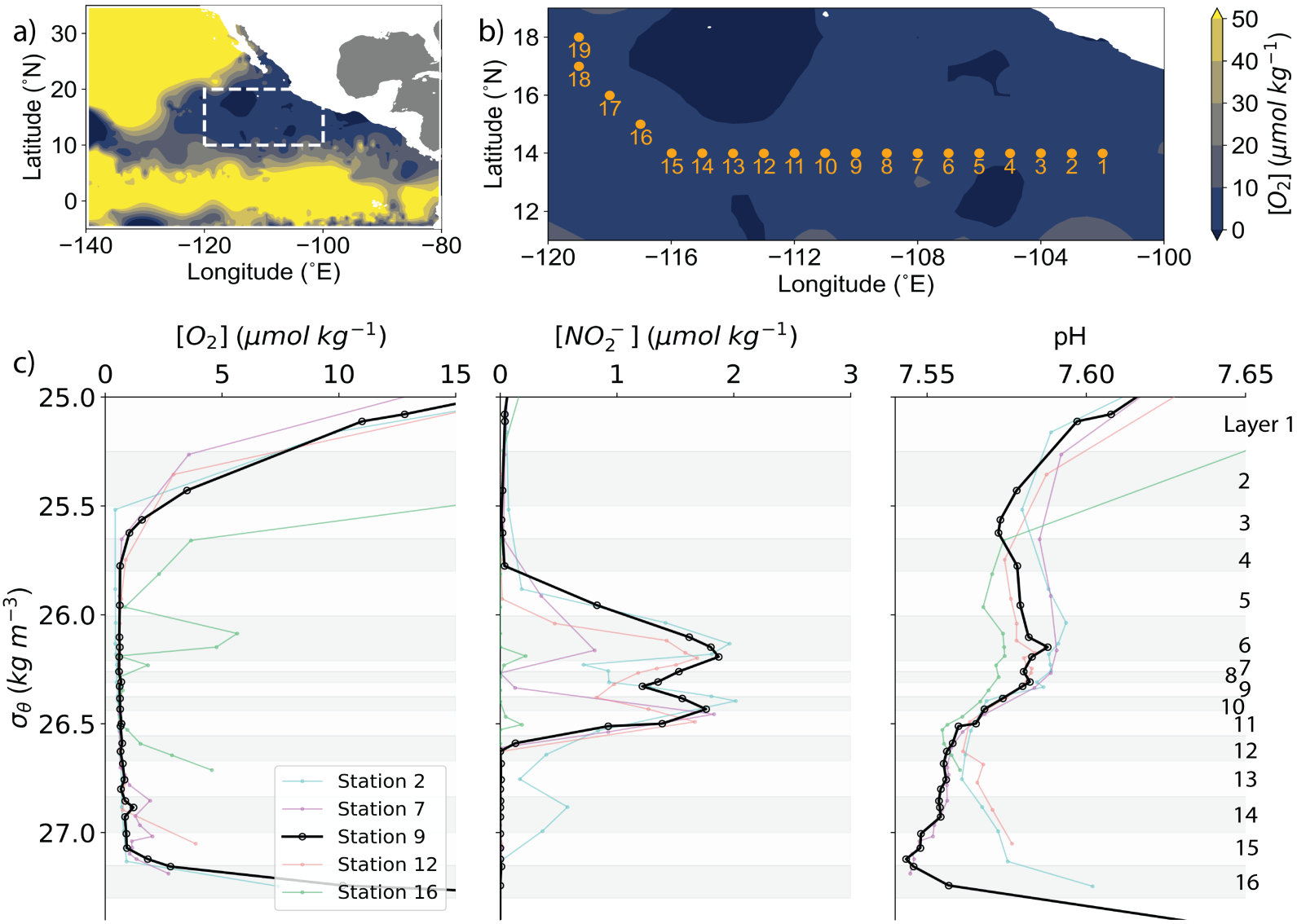
a)
Latitude (°N)
Longitude (°E)
b)
Latitude (°N)
Longitude (°E)
[O2] (μmol kg−1)
c)
[O2] (μmol kg−1)
[NO2−] (μmol kg−1)
pH
σθ (kg m−3)
Station 2
Station 7
Station 9
Station 12
Station 16
Layer 1

Figure 3.

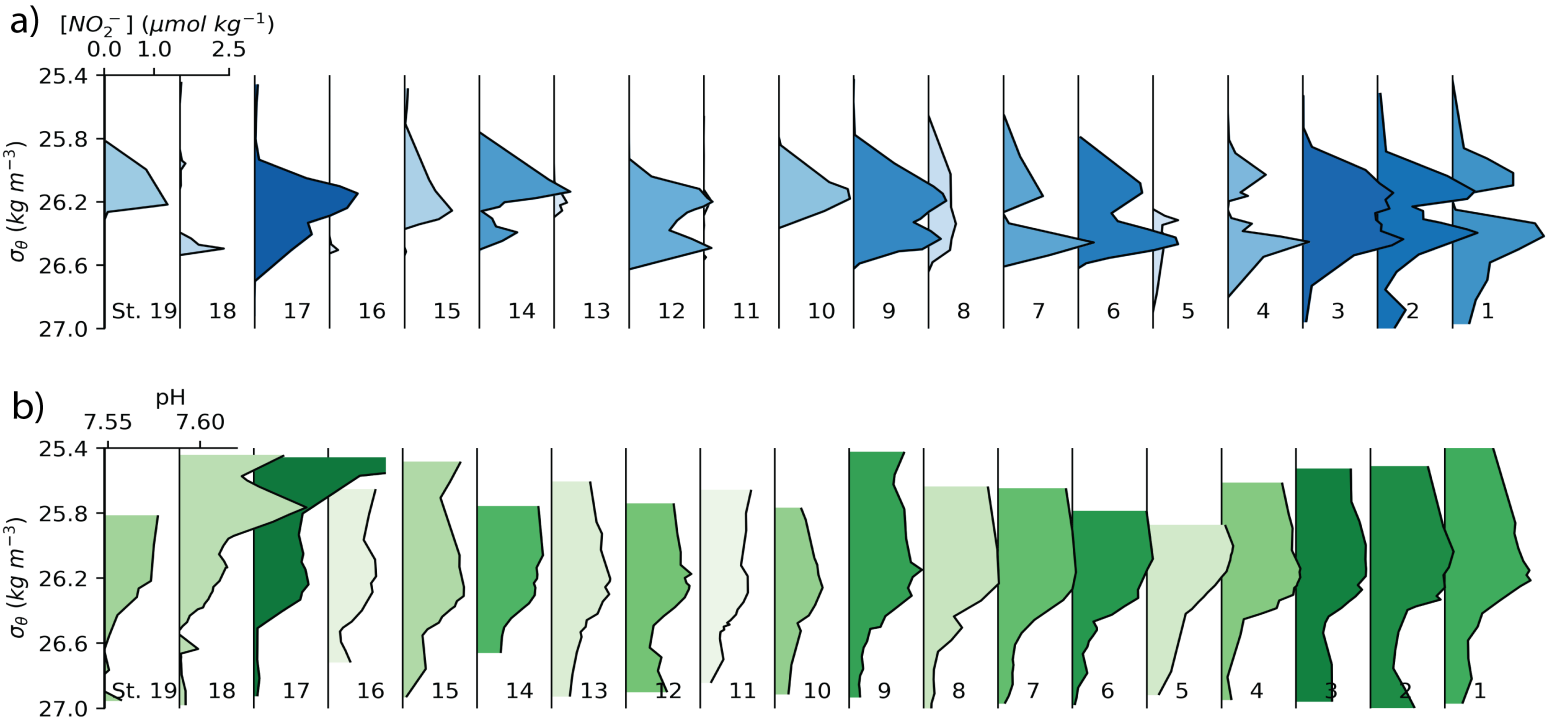
a)
$[NO_2^-]$ ($\mu mol\ kg^{-1}$)
0.0 1.0 2.5
25.4
25.8
26.2
26.6
27.0
σ_θ ($kg\ m^{-3}$)
St. 19 18 17 16 15 14 13 12 11 10 9 8 7 6 5 4 3 2 1
b)
pH
7.55 7.60
25.4
25.8
26.2
26.6
27.0
σ_θ ($kg\ m^{-3}$)
St. 19 18 17 16 15 14 13 12 11 10 9 8 7 6 5 4 3 2 1

Figure 4.

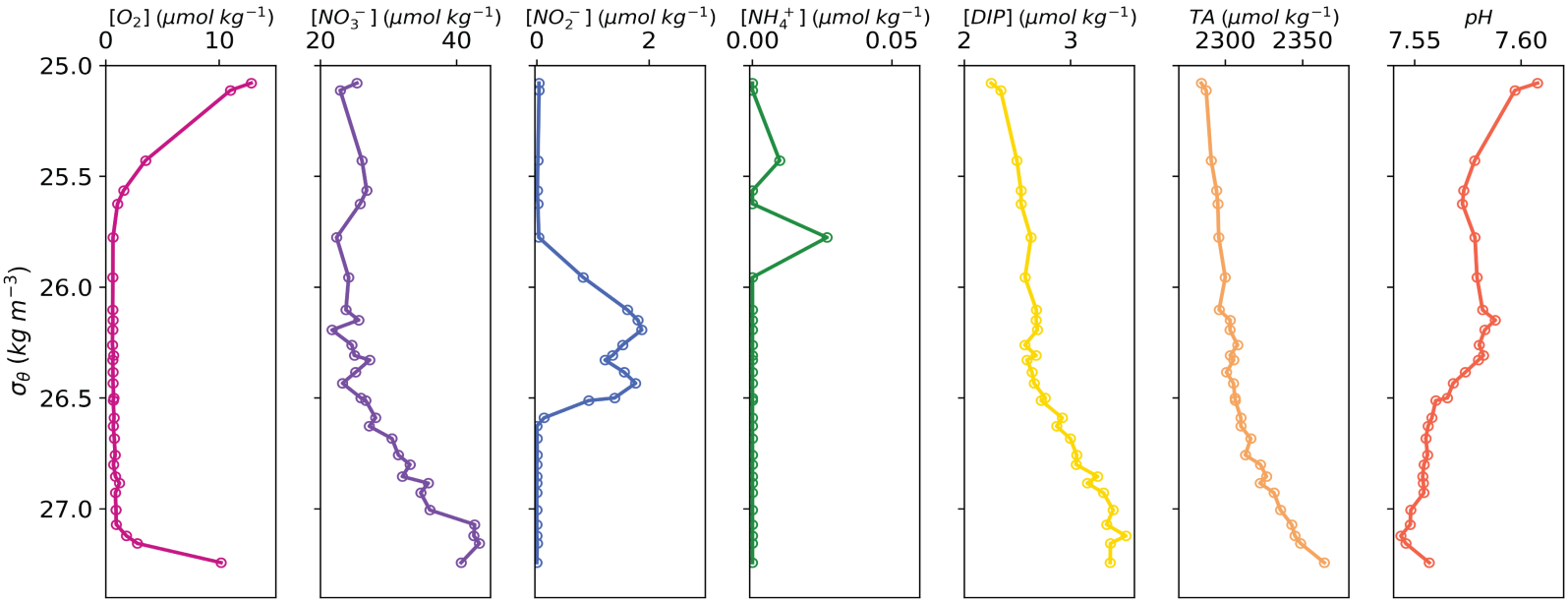
[O_2] ($\mu mol\ kg^{-1}$)
0
10
[NO_3^-] ($\mu mol\ kg^{-1}$)
20
40
[NO_2^-] ($\mu mol\ kg^{-1}$)
0
2
[NH_4^+] ($\mu mol\ kg^{-1}$)
0.00
0.05
[DIP] ($\mu mol\ kg^{-1}$)
2
3
TA ($\mu mol\ kg^{-1}$)
2300
2350
pH
7.55
7.60
25.0
25.5
26.0
26.5
27.0
σ_θ ($kg\ m^{-3}$)

Figure 5.

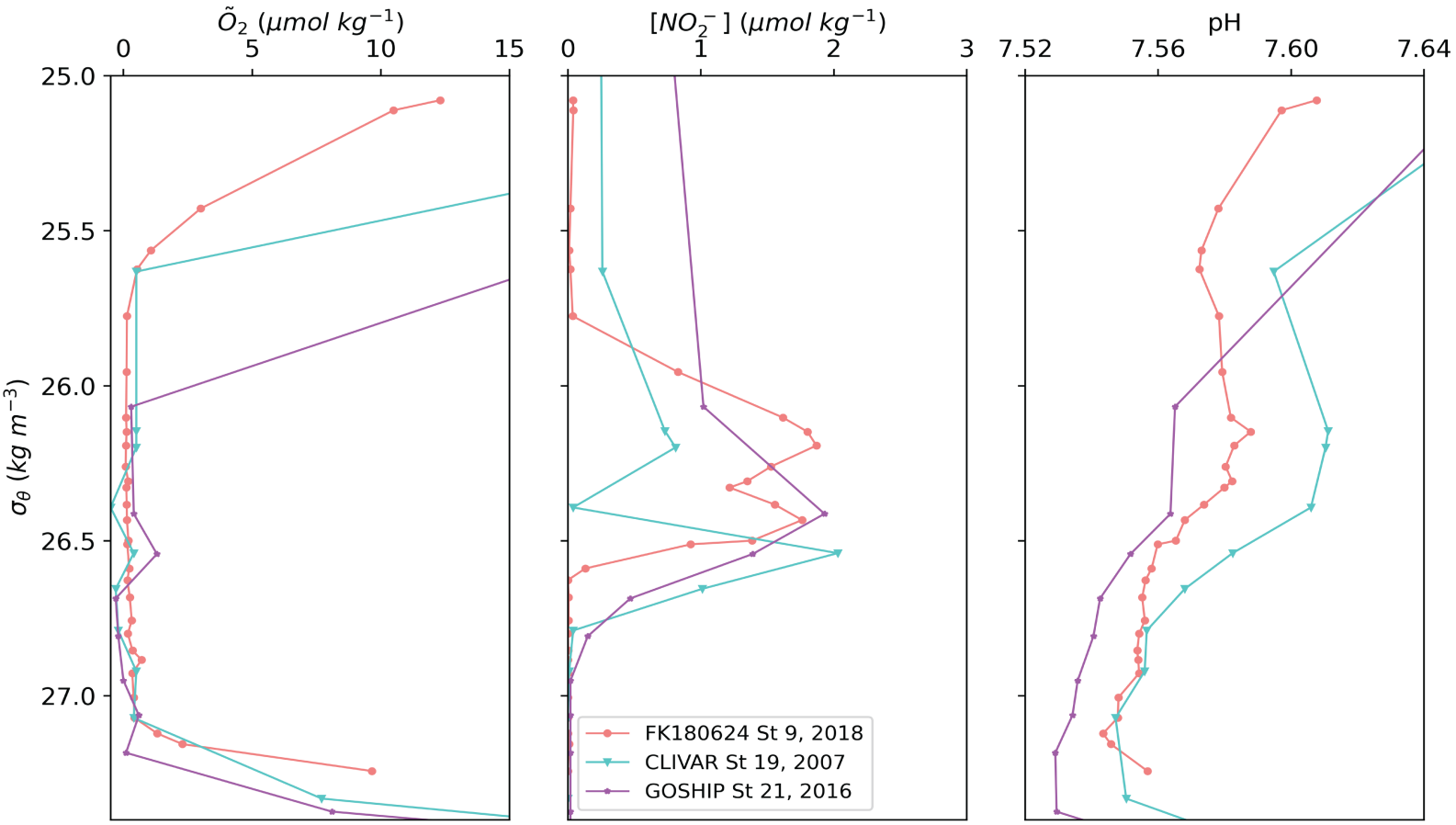
$\tilde{O}_2$ ($\mu mol\ kg^{-1}$)
0
5
10
15
$[NO_2^-]$ ($\mu mol\ kg^{-1}$)
0
1
2
3
pH
7.52
7.56
7.60
7.64
25.0
25.5
26.0
26.5
27.0
σ_θ ($kg\ m^{-3}$)
FK180624 St 9, 2018
CLIVAR St 19, 2007
GOSHIP St 21, 2016

Figure 6.

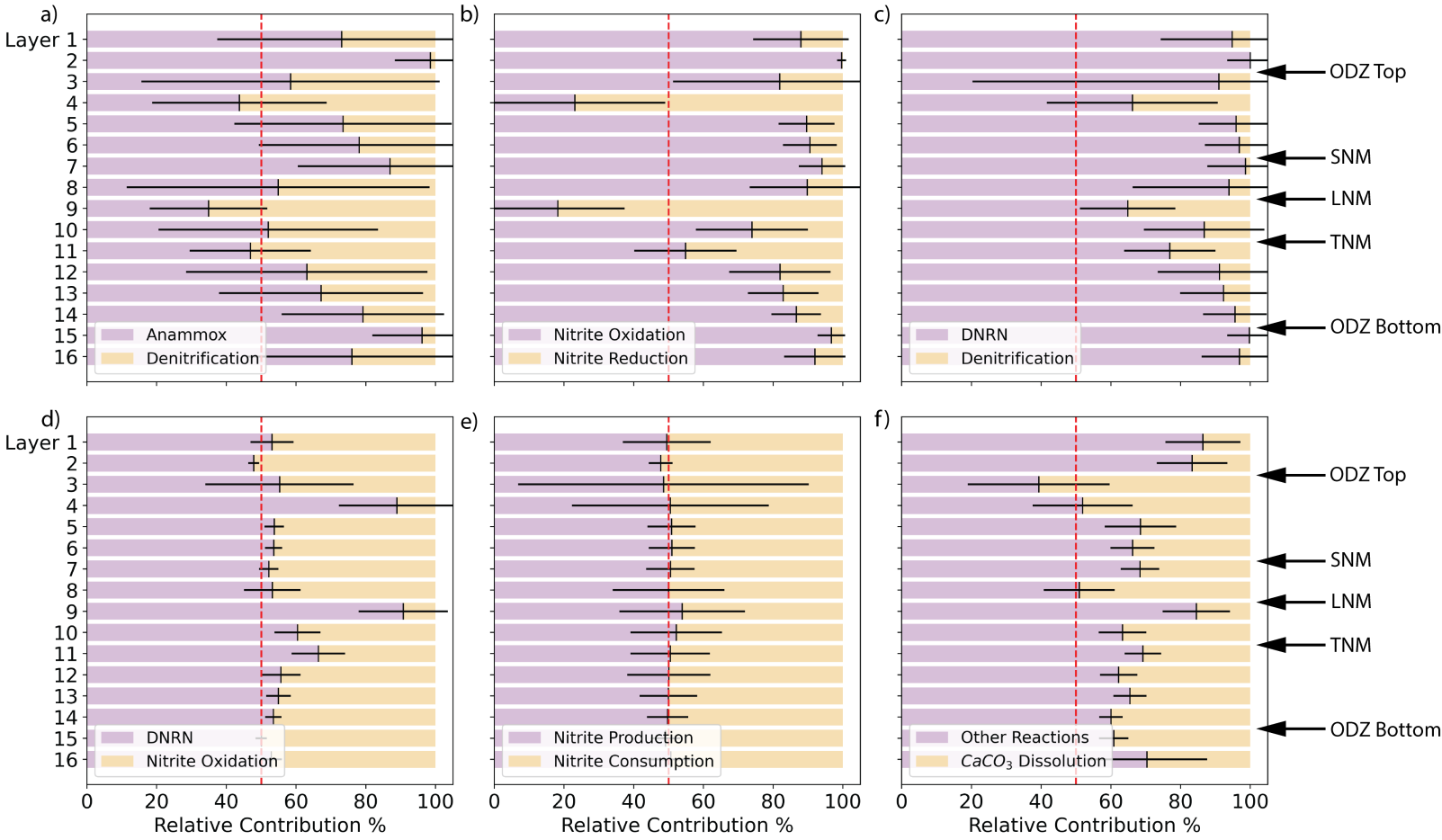
a)
b)
c)
d)
e)
f)
Layer 1
2
3
4
5
6
7
8
9
10
11
12
13
14
15
16
Anammox
Denitrification
Nitrite Oxidation
Nitrite Reduction
DNRN
Denitrification
DNRN
Nitrite Oxidation
Nitrite Production
Nitrite Consumption
Other Reactions
$CaCO_3$ Dissolution
ODZ Top
SNM
LNM
TNM
ODZ Bottom
0
20
40
60
80
100
Relative Contribution %

Figure 7.

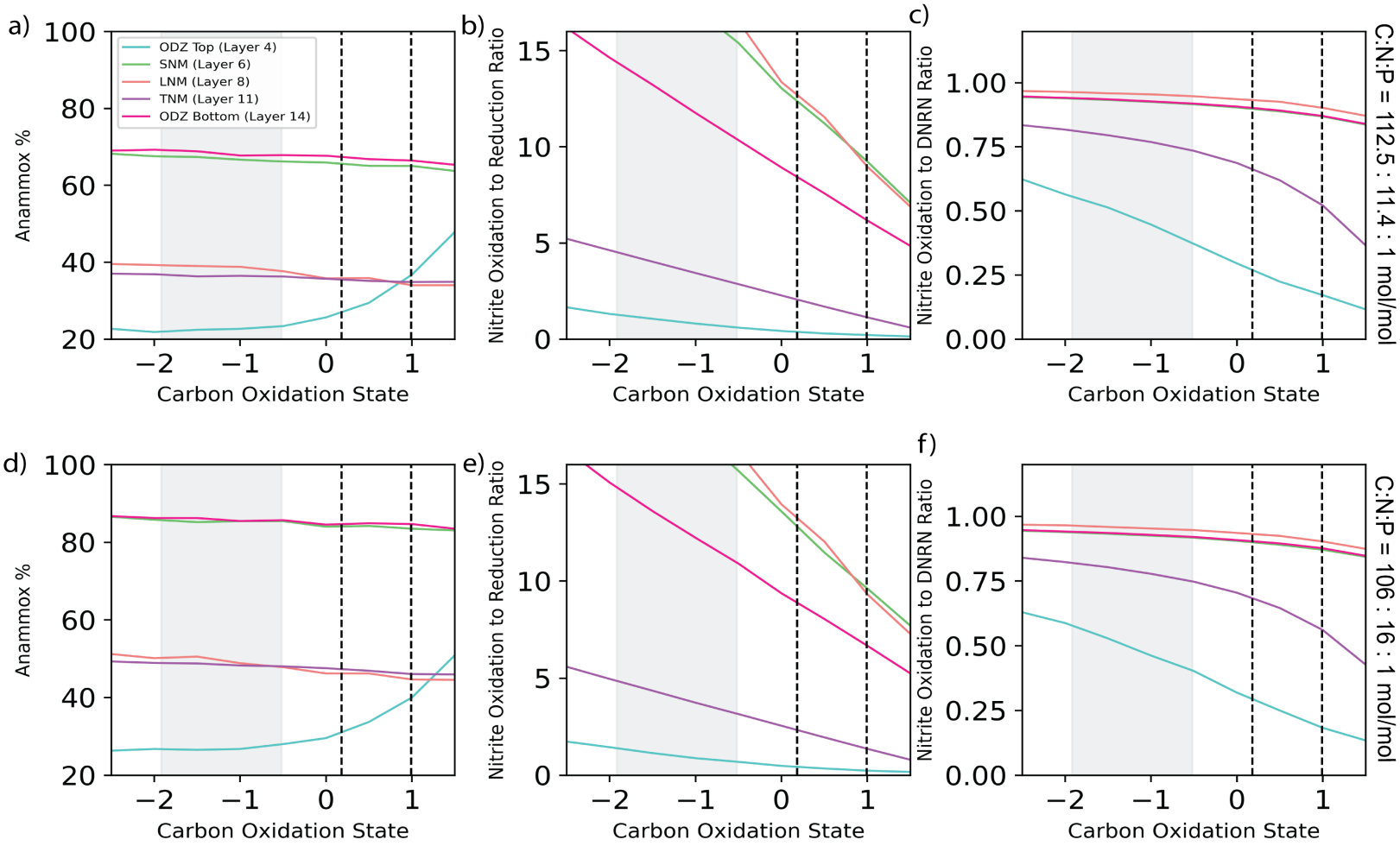
a)
b)
c)
d)
e)
f)
ODZ Top (Layer 4)
SNM (Layer 6)
LNM (Layer 8)
TNM (Layer 11)
ODZ Bottom (Layer 14)
Anammox %
Nitrite Oxidation to Reduction Ratio
Nitrite Oxidation to DNRN Ratio
Carbon Oxidation State
C:N:P = 112.5 : 11.4 : 1 mol/mol
C:N:P = 106 : 16 : 1 mol/mol

Figure 8.

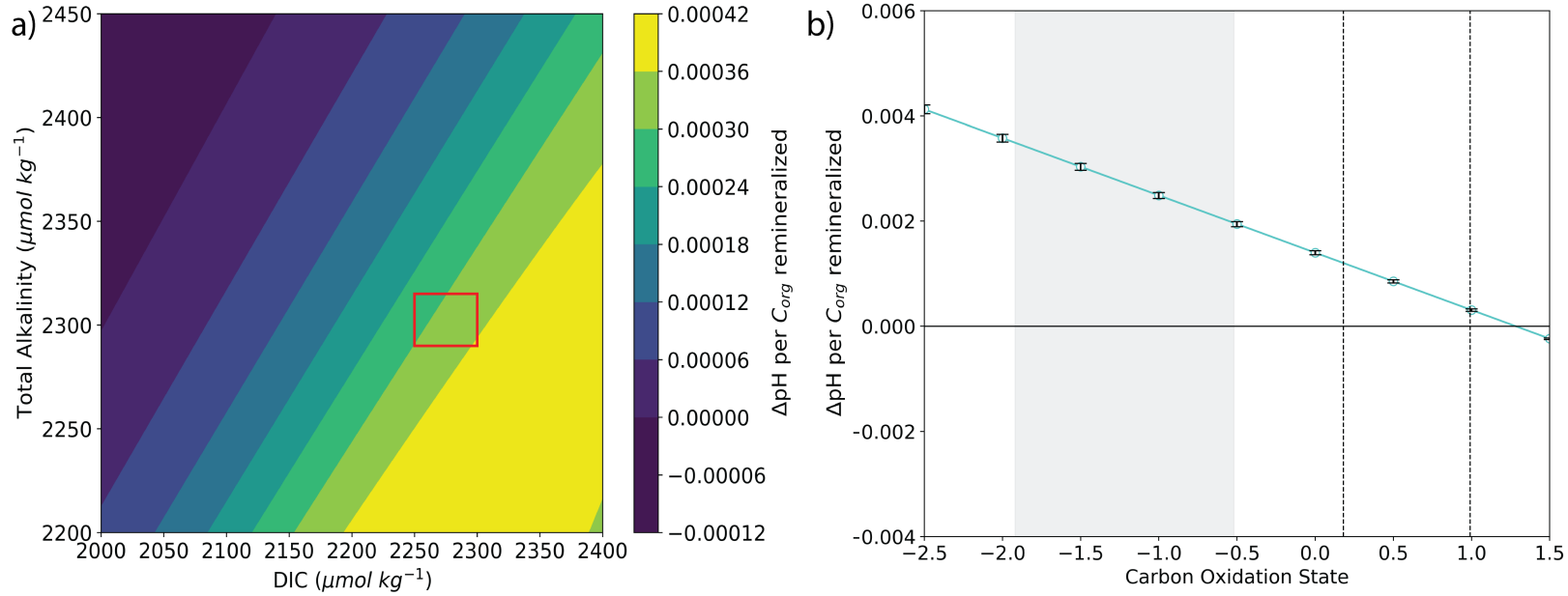
a)
Total Alkalinity ($\mu mol\ kg^{-1}$)
DIC ($\mu mol\ kg^{-1}$)
ΔpH per C_{org} remineralized
b)
ΔpH per C_{org} remineralized
Carbon Oxidation State

Figure 9.

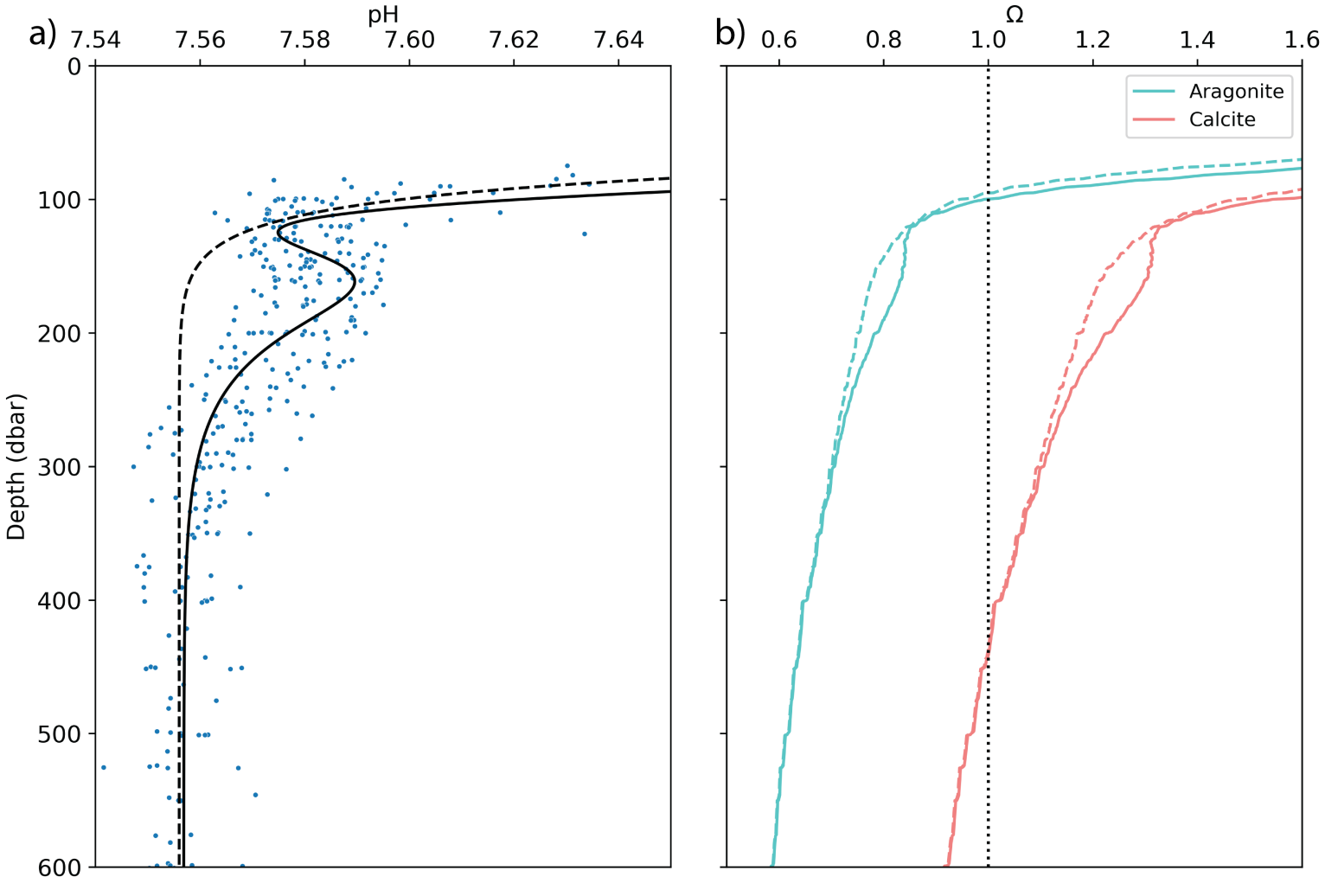
a)
pH
7.54
7.56
7.58
7.60
7.62
7.64
Depth (dbar)
0
100
200
300
400
500
600
b)
Ω
0.6
0.8
1.0
1.2
1.4
1.6
Aragonite
Calcite

Table 1

Process	Chemical Reaction
DNRN	$OM + xNO_3^- + dH^+ \rightarrow a\,CO_2 + d\,NH_4^+ + eH_3PO_4 + xNO_2^- + yH_2O$
Denitrification	$OM + zNO_2^- + (z+d)H^+ \rightarrow a\,CO_2 + dNH_4^+ + eH_3PO_4 + \frac{z}{2}\,N_2 + wH_2O$
Anammox	$NH_4^+ + 1.32\,NO_2^- + 0.11\,CO_2 + 0.02\,H^+ \rightarrow\ N_2 + 0.11\,OM^{amx} + 1.90H_2O + 0.3NO_3^-$
Nitrite Oxidation	$NO_2^- + Oxidiant \rightarrow NO_3^- + Reductant$
$CaCO_3$ Dissolution	$CaCO_3 \rightarrow Ca^{2+} + CO_3^{2-}$

Note. $C_{ox} = 4 - \frac{4[(r_{AOU:P}) - 2d]}{a}$, $(b - 2c) = (3d\ -\ a * C_{ox} - 5e)$, $x = [2a + 0.5(b - 2c) - 1.5d + 2.5e]$, $y = [0.5b - 1.5d - 1.5e]$, $z = [\frac{4}{3}a + \frac{1}{3}(b - 2c) - d + \frac{5}{3}e]$, $w = [\frac{2}{3}a + \frac{2}{3}b - \frac{1}{3}c - 2d - \frac{2}{3}e]$

Table 2

Tracer	DNRN	Denitrification	Anammox	Nitrite Oxidation	$CaCO_3$ Dissolution
ΔNO_3^-	-1.505	0.000	2.909	46.296	0.000
ΔNO_2^-	+1.505	-1.003	-12.000	-46.296	0.000
ΔNH_4^+	0.101	0.101	-9.091	0.000	0.000
ΔN*	0.000	-1.003	-18.182	0.000	0.000
ΔTA	0.092	1.096	0.181	0.000	2.000
ΔDIC	1.000	1.000	-1.000	-1.000	1.000